Fig. 6. The specific interaction of MyD88 with TIRAP is independent of the conformational characteristics of the TIR domain. (A) HEK293TCM cells [17] were co-transfected with 10 ng of NF-κB reporter construct and the expression plasmids for the indicated combinations of empty vector (0.7 or 0.8 µg), MyD88 (0.1 µg), TRIFTIR (0.1 µg), and TLR4-YFP (2 ng). After 24 h, NF-κB-dependent luciferase activity was measured. Results are shown as the means ± standard deviation of three independent experiments. (B) GST pull-down assay. GST fusion proteins were incubated with lysates prepared from HEK293T cells transfected with empty vector or TIRAP-FLAG. The interaction of TIRAP with GST fusion proteins was detected by immunoblotting with anti-FLAG antibody. (C) Coomassie blue staining to detect GST-MyD88, GST-TRIFTIR, and GST proteins purified from bacteria. (D) Lysates from 293TCM-TLR4-YFP cells transfected with the indicated expression plasmids were subjected to co-immunoprecipitation analysis as described in Fig. 5. The asterisks next to the upper and the middle panels show the immunoglobulin light chain of anti-HA antibody used in the immunoprecipitation.

(14.1 ± 2.4-fold increase). These results suggest that the TRIF-TIR mutant mediates TLR4 signaling. To test whether the TRIFTIR mutant is required to physically interact with TIR-AP to mediate TLR4 signaling, we performed a GST pull-down assay. TIRAP interacted with the GST-TRIFTIR mutant more efficiently than with the GST-MyD88 proteins (Fig. 6B). Coomassie blue staining confirmed that the same amounts of GST-fusion proteins were used in the assay (Fig. 6C). Furthermore, we investigated the interaction of TIRAP and the TRIFTIR mutant using co-immunoprecipitation analysis. Consistent with the results from the GST pull-down assay, TIRAP co-immunoprecipitated more efficiently with the TRIFTIR mutant than with wild-type MyD88 in HEK293TCM-TLR4-YFP cells (Fig. 6D). These results suggest that the affinity of the TIR domain of TRIF for TIRAP may be stronger than that for MyD88. It is likely that the MyD88-TIRAP interaction required for TLR4 signaling is independent of the conformational characteristics of the TIR domain.

Although our results showed a physical interaction between the TRIFTIR mutant and TIRAP, TRIF itself does not interact with TIRAP. Similar to TLRs, the TIR adaptors exhibit a notably diverse subcellular distribution. TRIF is diffusely expressed in the cytoplasm [12], whereas TIRAP and TRAM are localized on or proximal to the plasma membrane owing to their targeting motifs, which include phosphatidylinositol 4,5-bisphosphate (PIP2)-binding domains and myristoylation sites [11,29]. Because the TRIFTIR mutant was co-localized with MyD88 (Fig. 3C), TRIF might interact with TIRAP if TRIF is targeted to a location in which MyD88 is enriched.

3.7. Concluding remarks

MyD88 is present in condensed, morphologically diverse forms in the cytoplasm. Our results demonstrate that the entire non-TIR region is sufficient for targeting MyD88 to as yet uncharacterized locations within the cell, where it interacts with signaling molecules and induces host defense responses. Furthermore, the interaction between MyD88 and specific TLRs is likely determined by the conformational characteristics of each TIR domain, whereas the specific interaction of MyD88 and TIRAP required for TLR4 signaling is likely determined by other spatiotemporal factors. These distinctive properties of the TIR and non-TIR regions are important for inducing effective immune responses via targeting MyD88 to the correct cellular location and by preventing MyD88 from associating with inappropriate partners.
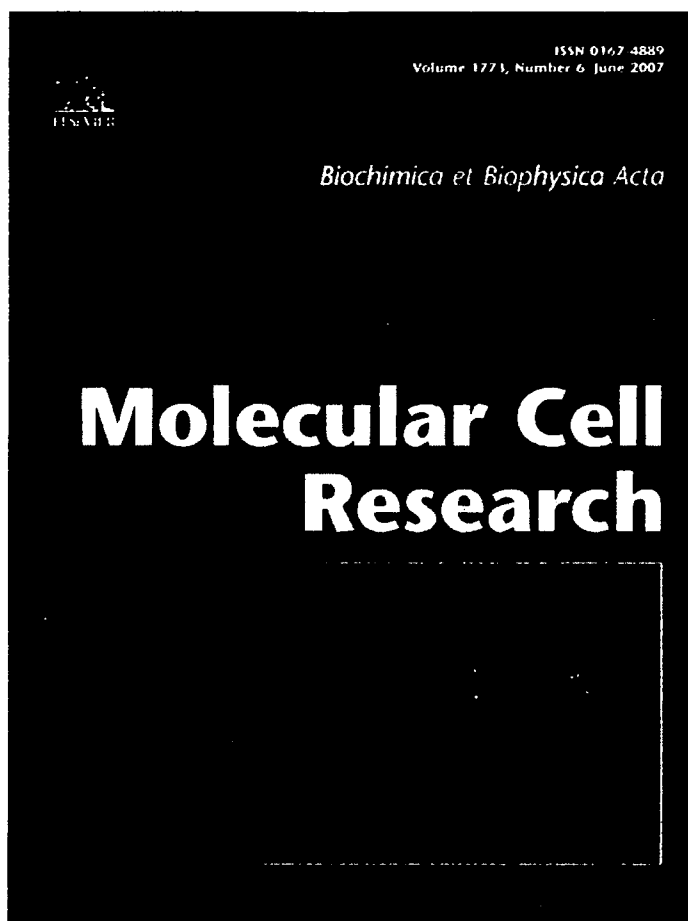
References

[1] Akira, S. and Takeda, K. (2004) Toll-like receptor signalling. Nat. Rev. Immunol. 4, 499–511.
[2] Akira, S., Uematsu, S. and Takeuchi, O. (2006) Pathogen recognition and innate immunity. Cell 124, 783–801.
[3] Wesche, H., Henzel, W.J., Shillinglaw, W., Li, S. and Cao, Z. (1997) MyD88: an adapter that recruits IRAK to the IL-1 receptor complex. Immunity 7, 837–847.

[4] Adachi, O., Kawai, T., Takeda, K., Matsumoto, M., Tsutsui, H., Sakagami, M., Nakanishi, K. and Akira, S. (1998) Targeted disruption of the MyD88 gene results in loss of IL-1- and IL-18-mediated function. Immunity 9, 143–150.

[5] Burns, K., Martinon, F., Esslinger, C., Pahl, H., Schneider, P., Bodmer, J.L., Di Marco, F., French, L. and Tschopp, J. (1998) MyD88, an adapter protein involved in interleukin-1 signaling. J. Biol. Chem. 273, 12203–12209.

[6] Medzhitov, R., Preston-Hurlburt, P., Kopp, E., Stadlen, A., Chen, C., Ghosh, S. and Janeway Jr., C.A. (1998) MyD88 is an adaptor protein in the hToll/IL-1 receptor family signaling pathways. Mol. Cell 2, 253–258.

[7] Kawai, T., Adachi, O., Ogawa, T., Takeda, K. and Akira, S. (1999) Unresponsiveness of MyD88-deficient mice to endotoxin. Immunity 11, 115–122.

[8] Jaunin, F., Burns, K., Tschopp, J., Martin, T.E. and Fakan, S. (1998) Ultrastructural distribution of the death-domain-containing MyD88 protein in HeLa cells. Exp. Cell Res. 243, 67–75.

[9] Kawai, T., Sato, S., Ishii, K.J., Coban, C., Hemmi, H., Yamamoto, M., Terai, K., Matsuda, M., Inoue, J., Uematsu, S., Takeuchi, O. and Akira, S. (2004) Interferon-alpha induction through Toll-like receptors involves a direct interaction of IRF7 with MyD88 and TRAF6. Nat. Immunol. 5, 1061–1068.

[10] Honda, K., Ohba, Y., Yanai, H., Negishi, H., Mizutani, T., Takaoka, A., Taya, C. and Taniguchi, T. (2005) Spatiotemporal regulation of MyD88-IRF-7 signalling for robust type-I interferon induction. Nature 434, 1035–1040.

[11] Kagan, J.C. and Medzhitov, R. (2006) Phosphoinositide-mediated adaptor recruitment controls Toll-like receptor signaling. Cell 125, 943–955.

[12] Honda, K., Yanai, H., Mizutani, T., Negishi, H., Shimada, N., Suzuki, N., Ohba, Y., Takaoka, A., Yeh, W.C. and Taniguchi, T. (2004) Role of a transductional–transcriptional processor complex involving MyD88 and IRF-7 in Toll-like receptor signaling. Proc. Natl. Acad. Sci. USA 101, 15416–15421.

[13] Verthelyi, D., Ishii, K.J., Gursel, M., Takeshita, F. and Klinman, D.M. (2001) Human peripheral blood cells differentially recognize and respond to two distinct CPG motifs. J. Immunol. 166, 2372–2377.

[14] Nishiya, T. and DeFranco, A.L. (2004) Ligand-regulated chimeric receptor approach reveals distinctive subcellular localization and signaling properties of the Toll-like receptors. J. Biol. Chem. 279, 19008–19017.

[15] Onishi, M., Kinoshita, S., Morikawa, Y., Shibuya, A., Phillips, J., Lanier, L.L., Gorman, D.M., Nolan, G.P., Miyajima, A. and Kitamura, T. (1996) Applications of retrovirus-mediated expression cloning. Exp. Hematol. 24, 324–329.

[16] Murai, K., Murakami, H. and Nagata, S. (1998) Myeloid-specific transcriptional activation by murine myeloid zinc-finger protein 2. Proc. Natl. Acad. Sci. USA 95, 3461–3466.

[17] Nishiya, T., Kajita, E., Miwa, S. and Defranco, A.L. (2005) TLR3 and TLR7 are targeted to the same intracellular compartments by distinct regulatory elements. J. Biol. Chem. 280, 37107–37117.

[18] Nishiya, T., Kajita, E. and Miwa, S. (2006) Ligand-independent oligomerization of TLR4 regulated by a short hydrophobic region adjacent to the transmembrane domain. Biochem. Biophys. Res. Commun. 341, 1128–1134.

[19] Petiot, A., Faure, J., Stenmark, H. and Gruenberg, J. (2003) PI3P signaling regulates receptor sorting but not transport in the endosomal pathway. J. Cell Biol. 162, 971–979.

[20] Hornef, M.W., Frisan, T., Vandewalle, A., Normark, S. and Richter-Dahlfors, A. (2002) Toll-like receptor 4 resides in the Golgi apparatus and colocalizes with internalized lipopolysaccharide in intestinal epithelial cells. J. Exp. Med. 195, 559–570.

[21] Latz, E., Schoenemeyer, A., Visintin, A., Fitzgerald, K.A., Monks, B.G., Knetter, C.F., Lien, E., Nilsen, N.J., Espevik, T. and Golenbock, D.T. (2004) TLR9 signals after translocating from the ER to CpG DNA in the lysosome. Nat. Immunol. 5, 190–198.

[22] Lee, J., Chuang, T.H., Redecke, V., She, L., Pitha, P.M., Carson, D.A., Raz, E. and Cottam, H.B. (2003) Molecular basis for the immunostimulatory activity of guanine nucleoside analogs: activation of Toll-like receptor 7. Proc. Natl. Acad. Sci. USA 100, 6646–6651.

[23] Leifer, C.A., Kennedy, M.N., Mazzoni, A., Lee, C., Kruhlak, M.J. and Segal, D.M. (2004) TLR9 is localized in the endoplasmic reticulum prior to stimulation. J. Immunol. 173, 1179–1183.

[24] Yamamoto, M., Sato, S., Mori, K., Hoshino, K., Takeuchi, O., Takeda, K. and Akira, S. (2002) Cutting edge: a novel Toll/IL-1 receptor domain-containing adapter that preferentially activates the IFN-beta promoter in the Toll-like receptor signaling. J. Immunol. 169, 6668–6672.

[25] Oshiumi, H., Matsumoto, M., Funami, K., Akazawa, T. and Seya, T. (2003) TICAM-1, an adaptor molecule that participates in Toll-like receptor 3-mediated interferon-beta induction. Nat. Immunol. 4, 161–167.

[26] Takeda, K. and Akira, S. (2005) Toll-like receptors in innate immunity. Int. Immunol. 17, 1–14.

[27] Fitzgerald, K.A., Palsson-McDermott, E.M., Bowie, A.G., Jefferies, C.A., Mansell, A.S., Brady, G., Brint, E., Dunne, A., Gray, P., Harte, M.T., McMurray, D., Smith, D.E., Sims, J.E., Bird, T.A. and O'Neill, L.A. (2001) Mal (MyD88-adapter-like) is required for Toll-like receptor-4 signal transduction. Nature 413, 78–83.

[28] Horng, T., Barton, G.M., Flavell, R.A. and Medzhitov, R. (2002) The adaptor molecule TIRAP provides signalling specificity for Toll-like receptors. Nature 420, 329–333.

[29] Rowe, D.C., McGettrick, A.F., Latz, E., Monks, B.G., Gay, N.J., Yamamoto, M., Akira, S., O'Neill, L.A., Fitzgerald, K.A. and Golenbock, D.T. (2006) The myristoylation of TRIF-related adaptor molecule is essential for Toll-like receptor 4 signal transduction. Proc. Natl. Acad. Sci. USA 103, 6299–6304.

Molecular Cell Research

ELSEVIER

OCTN2VT, a splice variant of OCTN2, does not transport carnitine because of the retention in the endoplasmic reticulum caused by insertion of 24 amino acids in the first extracellular loop of OCTN2

Satoshi Maekawa [a,1], Daisuke Mori [a,1], Tadashi Nishiya [a,1], Osamu Takikawa [b],
Takahiro Horinouchi [a], Arata Nishimoto [a], Emi Kajita [a], Soichi Miwa [a,*]

[a] Department of Pharmacology, Hokkaido University Graduate School of Medicine, Sapporo 060-8638, Japan
[b] Laboratory of Radiation Safety, National Institute for Longevity Sciences, National Center for Geriatrics and Gerontology, Aichi 4740-8522, Japan

Abstract

A novel organic cation transporter OCTN2 is indispensable for carnitine transport across plasma membrane and subsequent fatty acid metabolism in the mitochondria. Here, we report a novel splice variant of OCTN2 (OCTN2VT), in which a 72-base-pair sequence located in the first intron of OCTN2 gene was spliced between exons 1 and 2 of OCTN2, causing the insertion of 24 amino acids in the first extracellular loop of OCTN2. Despite the similarity between OCTN2 and OCTN2VT regarding primary structure and tissue distribution, their biochemical characteristics were significantly different. OCTN2 was expressed on the plasma membrane with robust N-glycosylation, whereas OCTN2VT was retained in the endoplasmic reticulum (ER) with poor N-glycosylation. In addition, the retention in the ER caused no carnitine uptake into the cells. These results demonstrate that the biochemical and functional characteristics of OCTN2VT are distinct from OCTN2 due to the insertion of 24 amino acids in the first extracellular loop.
© 2007 Elsevier B.V. All rights reserved.

Keywords: OCTN2; OCTN2VT; Splicing; Carnitine; N-glycosylation; Endoplasmic reticulum

1. Introduction

Carnitine (β-hydroxy-γ-trimethylamino butyrate) is essential for transfer of long chain fatty acids from the cytosol to the mitochondrial matrix for subsequent β-oxidation to generate cellular energy [1]. The carnitine transport across the plasma membrane is mediated by novel organic cation transporter (OCTN) family proteins [2]. Three different OCTNs (OCTN1, OCTN2, and OCTN3) have been identified in humans and mice [3,4]. Among the OCTN family, OCTN2 has been shown to transport carnitine most efficiently, and malfunction of OCTN2 causes the primary systemic carnitine deficiency characterized by progressive cardiomyophathy, skeletal muscle myopathy, and hypoglycemia in humans [5]. The mice having a point mutation in

OCTN2 have severe disturbance of energy generation, causing serious symptoms in the heart and skeletal muscles, in which fatty acids are a primary source for energy [6]. Therefore, OCTN2 is indispensable for energy homeostasis in the body.

The biochemical properties and physiological functions of OCTN2 have been well established. OCTN2 transports carnitine in a Na^+-dependent manner [7]. OCTN2 is a twelve membrane-spanning protein with three putative N-glycosylation sites (Asn-57, -64, and -91) within the first extracellular loop [2]. Those sites are conserved in all members of an OCTN family [8], suggesting that OCTN2 enters the secretory pathway including endoplasmic reticulum (ER) and Golgi apparatus to be expressed on the plasma membrane.

Recently, we identified a novel up-regulator of OCTN2, cartregulin, in the rat brain [9]. Cartregulin is homologous to OCTN2, and upregulates the expression level of OCTN2 by stabilizing the mRNA of OCTN2. We also found a novel gene homologous to OCTN2 by searching the human genome database "the Assembled

---

* Corresponding author. Tel.: +81 11 706 6919; fax: +81 11 706 7824.
  E-mail address: smiwa@med.hokudai.ac.jp (S. Miwa).
  [1] These authors contributed equally to this work.

EST (AssEST)". This gene encodes a full-length OCTN2 with the insertion of 24 amino acids (QDSGAYNAMKNRMGKKPALCL-PAQ) between Glu-131 and Trp-132 in the first extracellular loop of OCTN2. This variant type of OCTN2 (designated as OCT N2VT) was expected to possess the biochemical and physiological characteristics similar to the OCTN2, because of the similarity between OCTN2 and OCTN2VT regarding the primary structure. However, the actual characteristics of OCTN2VT and the mechanism by which OCTN2VT is produced are unknown.

In the present study, we attempted to elucidate these issues by using HeLa cells stably expressing the yellow fluorescent protein (YFP)-tagged OCTN2VT. We found that despite the similar expression profiles in the human tissues between OCTN2 and OCTN2VT, their biochemical characteristics were significantly different. That is, (1) OCTN2 was highly N-glycosylated and expressed on the cell surface, whereas OCTN2VT was retained in the ER without N-glycosylation; (2) OCTN2VT-expressed HeLa cells could not take up carnitine due to the absence of OCTN2VT on the plasma membrane; (3) the DNA sequence encoding the 24 amino acids inserted in the OCTN2VT was located in the first intron of OCTN2 genome with being interposed between the GU-AG intron termini, suggesting the mechanism of the splicing to generate the OCTN2VT protein. Taken together, these results demonstrate that OCTN2VT, a novel

splice variant of OCTN2, is biochemically and functionally distinct from OCTN2 and other OCTN family proteins.

2. Materials and methods

2.1. Reagents and cell culture

Anti-GFP antibody (A.v. monoclonal antibody: clone JL-8) and anti-KDEL antibody were purchased from Clontech (Mountain View, CA) and Stressgen (Ann Arbor, MI), respectively. Peptide N-Glycosidase F (PNGase F) was purchased from New England Biolabs (Beverly, MA). L-[methyl-^{3}H]Carnitine HCl was purchased from Amersham Biosciences (Sydney, Australia). HeLa cells were grown in Dulbecco's modified Eagle's medium supplemented with 10% fetal bovine serum.

2.2. PCR analysis

PCR was carried out by using human kidney cDNA library (Stratagene, La Jolla, CA) as a template for 35 cycles (94 °C for 15 s, 55 °C for 30 s, and 72 °C for 2 min). Four types of primer designated primer a, b, c, and d were used (Fig. 1C). Primer a (5'-CATGCGGGAGTACGACGAGGTGACC-3') and primer d (5'-TCTTTCCTCTTCAGTTTCTCCCTTA-3') correspond to 5'- and 3'-ends of OCTN2, respectively. Primer b (5'-GGCTTCTTTCCCATCCTGTTTTTCA-3') and primer c (5'-TACAATGCTATGAAAAACAGGATGG-3') are reverse and forward primers, respectively, corresponding to 3'- and 5'-ends of the insert specific for OCTN2VT. The PCR products were subjected to gel electrophoresis to determine the sizes of the products.

A

```
                                          TM1
OCTN2    1 MRDYDEVTAF LGEWGPFQRL IFFLLSASII PNGFTGLSSV FLIATPEHRC
OCTN2VT  1 MRDYDEVTAF LGEWGPFQRL IFFLLSASII PNGFTGLSSV FLIATPEHRC
                    *          *
        51 RVPDAANLSS AWRNHTVPLR LRDGREVPHS CRRYRLATTA NFSALGLEPG
        51 RVPDAANLSS AWRNHTVPLR LRDGREVPHS CRRYRLATTA NFSALGLEPG
              *       *                                    *
       101 RDVDLGQLEQ ESCLDGWEFS QDVYLSTIVT E---------- ----------
       101 RDVDLGQLEQ ESCLDGWEFS QDVYLSTIVT EQDSGAYNAM KNRMGKKPAL
                                          TM2              TM3
       132 -----WNLVC EDDWKAPLTI SLFFVGVLLG SFISGQLSDR FGRKNVLFVT···· 557
       151 LLPAQWNLVC EDDWKAPLTI SLFFVGVLLG SFISGQLSDR FGRKNVLFVT···· 581
```

B

Intron 1   Intron 2

```
· · · · GGCCTGAACCCCACTGAGCGAGGGTGCCCTGCCTCTTCCACAGCCCTGGGCTCCG   Intron 1
CTCAGATTTTTAGGAGCAAGCGTTAGAGGCCTTGCTTTCTCCAGGGTCAGCATGTGGACA    (8,022 bp)
GAACACTTACTCTCTGCCTGTCTCTCCTCCTCAAAATGCAAGCAAGACAGTGGGGCCTAC
AATGCTATGAAAAACACGGATGGGAAAGAAGCCTGCTCTCTGCCTTCCTGCCCAGGTGAGC
CATCACCTGACTAAGTGAGTTCACACTCAGAGCGTGTGGGGATGGCAGGATGTTCTGACT
TCATTTTCCAGGATGCCTTTGCTTTAAAACCTTTTAAAAAGAAGTGAATGATACACCCCC
TTTGCTCATCTTGCAGTGCAACCTGGTGTGTGAGGACGACTGGAAGGCCCCACTCACAAT   Exon 2
CTCCTTGTTCTTCGTGGGTGTGCTGTTGGGCTCCTTCATTTCAGGGCAGCTGTCAGACAG
GTAAGGTGTCTGTCTTCTGGAGCACCAGGGGACCTCAGCACTGAGGAAGAAGCCGTGTGCC   Intron 2
TGGCCCTTGATTTCAGTTGGTAGTATTCTTTCAGCGCAGGGCCCTGTATTTTAAA·····   (5,668 bp)
```

C   **D**

```
      434 bp
   a→ ──── ←b
   ─────────────────
   c→ ────  1,360 bp  ←d
(kbp)
2.0 ─
1.5 ─         ←cd          OCTN2VT
1.0 ─
0.75─
0.5 ─    ←ab              β-actin
```
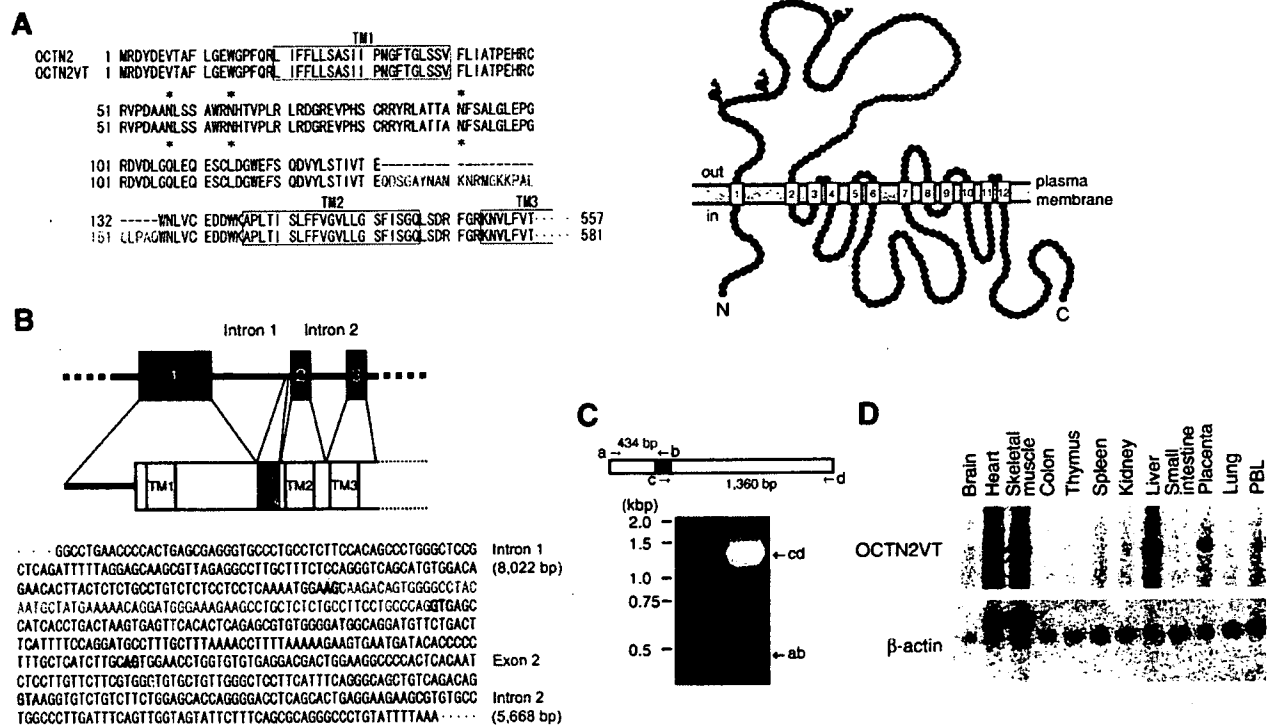
Fig. 1. Identification of a splice variant of OCTN2. (A) Alignment of OCTN2 and OCTN2VT proteins. The insertion of 24 amino acids in the OCTN2VT is shown in red in both amino acid sequence and the predicted secondary structure. The protein encoded by exon 2 is shown in blue. The three putative N-glycosylation sites are indicated by asterisks. The putative transmembrane domains (TM1, TM2, and TM3) are shown in boxes. (B) OCTN2VT generated from splicing of OCTN2 gene is illustrated. The genome sequence corresponding to the illustration is shown below. The DNA sequences of the spliced region and exon 2 are shown in red and blue, respectively. The GT-AG intron termini are shown in orange box. (C) Expression of OCTN2VT mRNA in the human kidney. Primers used for RT-PCR are shown by arrows. Primers b and c are specific for OCTN2VT cDNA. (D) Tissue distribution of OCTN2VT mRNA detected by northern blot analysis. (For interpretation of the references to colour in this figure legend, the reader is referred to the web version of this article.)

2.3. Northern blot analysis

Northern blot analysis was done using MTN Multiple Tissue Northern Blot (Human 12-Lane, Clontech, Mountain View, CA) as described previously [9]. A 72-bp fragment specific for OCTN2VT was used as a probe.

2.4. DNA constructs

The cDNAs encoding human OCTN2 and OCTN2VT were amplified by PCR from the human kidney cDNA library. The N91Q mutation was introduced by PCR-based site directed mutagenesis. Primers used here were 5′-CCACCA-TCGCCCAGTTCTCGGCGCT-3′ and 5′-AGCGCCGAGAACTGGGC-GATGGTGG-3′). The retroviral vectors for YFP-tagged OCTN2, OCTN2VT, and OCTN2(N91Q) were constructed as described previously [10].

2.5. Analysis of expression level by flow cytometry and immunoblotting

Introduction of $OCTN2^{YFP}$, $OCTN2VT^{YFP}$, and $OCTN2(N91Q)^{YFP}$ into HeLa cells was carried out by retroviral gene transfer as described previously [11]. The cells stably expressing $OCTN2^{YFP}$, $OCTN2VT^{YFP}$, or $OCTN2(N91Q)^{YFP}$ were selected by 2 μg/ml puromycin for 3 days. The expression levels of $OCTN2^{YFP}$, $OCTN2VT^{YFP}$, and $OCTN2(N91Q)^{YFP}$ were determined by flow cytometric analysis as described previously [11]. More than 95% of the cells expressed those proteins. The whole cell lysates were prepared as described previously [12]. All samples were loaded on gels without being boiled, because OCTN2 and OCTN2VT were highly aggregated by the sample-boiling step. The membrane fractions were prepared as described in Takaesu et al. [13]. The protein concentration of each fraction was measured with the Bio-Rad Protein Assay kit (Bio-Rad, Hercules, CA). Equal amounts of protein were loaded in each lane and separated by SDS-polyacrylamide gel electrophoresis. Gels were transferred onto Immobilon-P membranes (Millipore, Bedford, MA), and blotted with anti-GFP antibody. In the case of PNGase F treatment, 3 μg of OCTN2 membrane fraction and 50 μg of OCTN2VT membrane fraction were treated with PNGase F for 1 h at 37 °C. Then, the whole proteins were loaded and separated by SDS-PAGE. In the case of MG132 treatment, HeLa cells retrovirally expressing OCTN2VT were treated with 10 μM MG132 for indicated periods, and then the whole cell lysates were prepared.

2.6. Microscopy

HeLa cells expressing $OCTN2^{YFP}$ or $OCTN2VT^{YFP}$ were plated onto a glass bottom dish (IWAKI, Japan). Next day, the cells were fixed and permeabilized with Cytofix/Cytoperm solution (BD Pharmingen, San Diego, CA). Then, the cells were treated with anti-KDEL antibody followed by Alexa Fluor 594-conjugated anti-mouse IgG antibody. After washes, subcellular distributions of $OCTN2^{YFP}$ and $OCTN2VT^{YFP}$ were analyzed by Bio-Rad MRC1024 laser scanning confocal microscope.

2.7. Transport study in HeLa cells

The transport activity of OCTN2, OCTN2VT, or OCTN2(N91Q) was measured as described previously [9]. In brief, HeLa cells stably expressing YFP (vector alone), $OCTN2^{YFP}$, $OCTN2VT^{YFP}$, $OCTN2(N91Q)^{YFP}$ in a 24-well plate were pre-incubated in 0.2 ml of transport buffer (TB) [125 mM NaCl, 4.8 mM KCl, 5.6 mM D-glucose, 1.2 mM $CaCl_2$, 1.2 mM KH_2PO_4, 1.2 mM $MgSO_4$, and 25 mM HEPES (pH 7.4)] for 10 min at 37 °C, and transport reaction was started by addition of 0.2 ml of TB containing 4 nM [^{3}H]carnitine (81 Ci/mmol). After 7 min, the reaction was terminated by aspiration of TB followed by five washes with 1 ml of ice-cold TB. The amount of [^{3}H]carnitine transported into the cells was counted with a liquid-scintillation counter after solubilization of the cells with 0.5 ml of 1% SDS in 0.2 N NaOH. Data were presented as means±SEM. A pair of means was compared with Student's t-test. Groups of data were subjected to a two-way analysis of variance (ANOVA), and when a significant F value was encountered, Newman–Keuls' multiple-range test was used to test for significant differences between treatment means. A probability level of $P < 0.05$ was considered statistically significant.

2.8. Genbank accession number

The accession number for human OCTN2VT is AB291606.

3. Results and discussion

3.1. Isolation and tissue distribution of OCTN2VT

We have recently found a cDNA sequence encoding a variant type of OCTN2 (OCTN2VT) in the database "AssEST", which is a clustered sequence database containing expressed sequence tags and mRNA sequences in the public domain for human, mouse, rat, and chicken. The putative open reading frame of OCTN2VT was composed of DNA sequence encoding the full-length OCTN2 protein with a DNA-insertion for 24-amino acids (QDSGAYNAMKNRMGKKPALCLPAQ). The insertion was located between Glu-131 and Trp-132 in the first extracellular loop of OCTN2 (Fig. 1A). We searched for the location of the DNA sequence encoding the 24 amino acids in the human genome and found that it was located in the first intron of OCTN2 gene at the chromosome 5 (Fig. 1B). Interestingly, this DNA sequence was interposed between AG and GT (GU in mRNA) dinucleotides, both of which are conserved sequences for splicing of mRNA precursors [14]. Because AG and GU dinucleotides of mRNA precursors are recognized by a spliceosome as a 3′- and 5′-ends of intron, respectively, it is likely that in some case, a spliceosome might recognize the DNA sequence encoding 24 amino acids as an additional exon, leading to an insertion of its DNA sequence between exon 1 and exon 2 to generate OCTN2VT mRNA.

To examine whether mRNA for OCTN2VT is actually expressed in human tissues, we performed PCR using human kidney cDNA library as a template and primers specific for OCTN2VT cDNA. We used two sets of primers: one set corresponds to 5′-end of OCTN2 cDNA and 3′-end of the insert (primers a and b), while the other set corresponds to 5′-end of the insert and 3′-end of OCTN2 cDNA (primers c and d). When these sets of primers were used, PCR products with the expected size were obtained, indicating that mRNA for OCTN2VT is actually expressed. Therefore, we isolated the full-length OCTN2VT cDNA from human kidney cDNA library with PCR. The sequence of the PCR product was completely the same as that of the putative OCTN2VT obtained from the AssEST database. The tissue distribution of OCTN2VT mRNA studied by northern blotting was similar to that of OCTN2 [2] except lower expression in the kidney, indicating that OCTN2VT mRNA is actually expressed in human tissues, and that its gene expression may be regulated in a similar manner to OCTN2.

3.2. OCTN2VT is not an N-glycosylated protein

The first extracellular loop of the OCTN2 is extremely large compared to other extracellular loops (Fig. 1B), and the putative N-glycosylation sites (Asn-57, -64, and -91) are present in this loop [2], suggesting that the first extracellular loop may be critical for the regulation of functional or biochemical properties of OCTN2. Therefore, these properties of OCTN2VT may be altered by the insertion of unique 24 amino acid sequence. First, we investigated the biochemical properties of the OCTN2VT in HeLa cells stably expressing $OCTN2^{YFP}$ or $OCTN2VT^{YFP}$. Interestingly, the expression level of OCTN2VT, which was

analyzed by fluorescent-activated cell sorter (FACS) using fluorescent intensity of YFP as an index, was approximately 10% of the level for OCTN2, despite using the same retroviral expression vector, pMXrmv5 [10] (Fig. 2A and B). The similar result was observed in the immunoblotting (Fig. 2C). Notably, detection of the OCTN2VT protein required a longer exposure time than that of OCTN2. Because degradation of many proteins is regulated by a ubiquitin-proteasome pathway, we examined whether the OCTN2VT was rapidly degraded by this pathway. As shown in Fig. 2D, MG132, a selective 26S proteasome inhibitor, had no effect on the protein level of the OCTN2VT up to 12 h after its addition, suggesting that the lower level of the OCTN2VT is not due to rapid degradation via the ubiquitin-proteasome pathway.

OCTN2VT was detected as a smaller protein (75 kDa) than OCTN2 (90 kDa) on SDS-PAGE (Fig. 2C), although the molecular weight of OCTN2VT calculated from its amino acid sequence is apparently larger than that of OCTN2 because of the insertion of 24 amino acids (Fig. 1A). Because OCTN2 possesses potential N-glycosylation sites on the first extracellular loop, its larger molecular weight on SDS-PAGE seems to be due to glycosylation of OCTN2. Thus, smaller molecular size of OCTN2VT in comparison with OCTN2 might be due to less or absent N-glycosylation of OCTN2VT.

To verify this point, we compared the apparent molecular weights of OCTN2 and OCTN2VT after treatment of protein extracts with PNGase F, an amidase that cleaves nearly all types of oligosaccharides from glycoproteins. As shown in a right
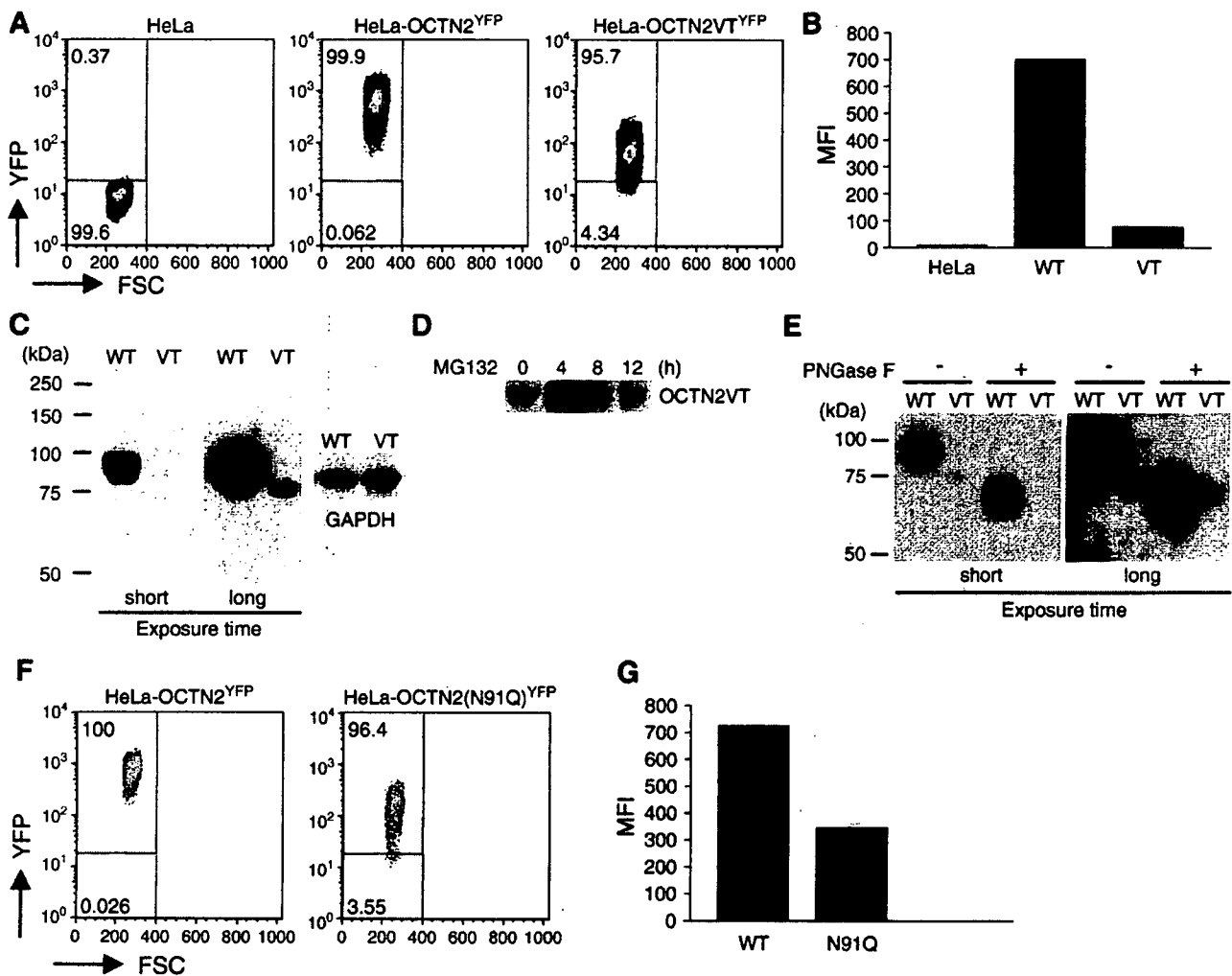

Fig. 2. Comparison of biochemical properties of OCTN2, OCTN2VT, and OCTN2(N91Q). (A) and (B) Expression levels of OCTN2 and OCTN2VT in HeLa cells following transfection of cDNA. OCTN2 and OCTN2VT tagged with YFP (designated OCTN2^YFP and OCTN2VT^YFP) were expressed in HeLa cells using retroviral vectors: in control cells, no transfection (designated HeLa). Fluorescent intensity of YFP in each cell was analyzed by FACS, and represented as a plot of fluorescent intensity in each cell (ordinate) against FSC (abscissa) (A) or mean fluorescent intensity (MFI) (B). (C) Immunoblot analysis of membrane fraction prepared from HeLa cells expressing OCTN2^YFP (WT) or OCTN2VT^YFP (VT) by anti-GFP antibody. Left and right panels represent the results with a short or long exposure time, respectively. (D) Immunoblot analysis for changes of expression level of OCTN2VT^YFP in HeLa cells following 4-h, 8-h, and 12-h treatment with 10 μM MG132, a proteasome inhibitor. (E) Immunoblot analysis as in panel C. Unlike panel C, membrane fractions prepared from HeLa cells expressing OCTN2^YFP (WT) and OCTN2VT^YFP (VT) were incubated with PNGase F for 1 h at 37 °C and subsequently subjected to SDS-PAGE. (F) and (G) Expression levels of OCTN2^YFP and OCTN2(N91Q)^YFP in HeLa cells following transfection of cDNA were analyzed by FACS.

panel of Fig. 2E, the apparent molecular weight of OCTN2 became markedly smaller after treatment with PNGase F (from 90 kDa to 75 kDa), whereas the change in the apparent molecular weight of OCTN2VT was very little. Consequently, after treatment with PNGase F, the apparent molecular weight of OCTN2 became nearly equal to that of OCTN2VT. These results taken together indicate that the different apparent molecular weights of OCTN2 and OCTN2VT reflect abundant glycosylation of OCTN2 and poor glycosylation of OCTN2VT. Because the insertion of 24 amino acids unique to OCTN2VT was located in the same loop as N-glycosylation sites, this insertion might block N-glycosylation in some way. To get insights into the relationship between N-glycosylation and expression level of OCTN2, we examined a mutant OCTN2 with one of the three potential N-glycosylation sites (Asn-91) being replaced by glutamine (OCTN2(N91Q)): this site was selected because it was the closest to the insertion of 24 amino acids. The expression level of this mutant was found to be reduced to about 50% of a wild type OCTN2 (Fig. 2F and G). These results taken together suggest that N-glycosylation may affect the expression level of OCTN2.

3.3. OCTN2VT is retained in the ER

During membrane trafficking for targeting to the plasma membrane, most proteins enter the secretory pathway, i.e. ER and Golgi apparatus, where the proteins are N-glycosylated [15]. Because OCTN2VT was minimally N-glycosylated (Fig. 2D),

there is the possibility that OCTN2VT cannot enter the secretory pathway and hence it cannot reach the plasma membrane. To test this possibility, we examined the subcellular localization of OCTN2 and OCTN2VT in HeLa cells stably expressing these molecules tagged with YFP. As shown in Fig. 3A, most of OCTN2 proteins were present on the cell surface, indicating that OCTN2 is expressed exclusively on the plasma membrane. In contrast, OCTN2VT proteins were present mainly in the cytoplasm, and its subcellular localization was found to be consistent with that of ER stained with anti-KDEL antibody, which specifically recognizes proteins localized to ER (Fig. 3B), suggesting that OCTN2VT is retained in ER. Since unglycosylated immature proteins are known to remain in ER to be subjected to proteolysis by the ER quality control system [16], it is likely that OCTN2VT which is lacking N-glycosylation is degraded rapidly because of its localization in ER.

3.4. OCTN2VT is a non-functional transporter for carnitine

To transport carnitine across the plasma membrane, OCTN family proteins must be expressed on the cell surface. However, since OCTN2VT was retained in the ER and not expressed on the cell surface (Fig. 3), it is assumed that OCTN2VT is non-functional as a transporter for carnitine. To test this, we measured the activity of carnitine transport in HeLa cells stably expressing OCTN2 and OCTN2VT. In comparison with the cells expressing OCTN2, the cells expressing OCTN2VT showed a very low but statistically significant level of carnitine transport activity: the
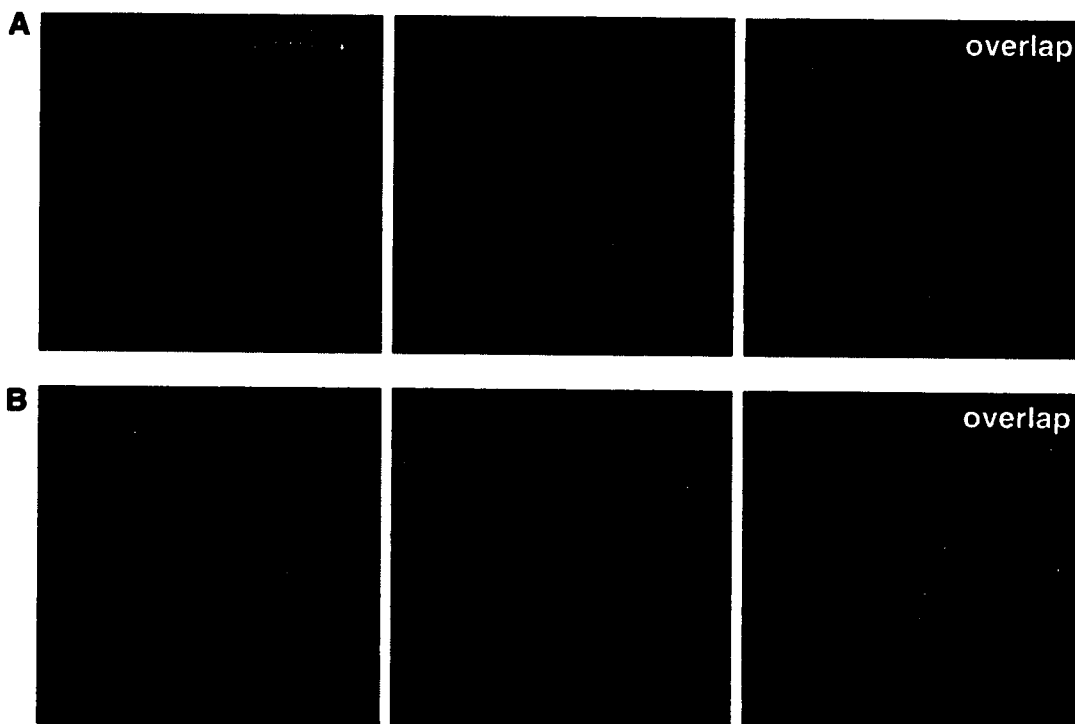

Fig. 3. Subcellular localization of OCTN2^{YFP} (A) and OCTN2VT^{YFP} (B). For staining of endoplasmic reticulum, HeLa cells expressing OCTN2^{YFP} and OCTN2VT^{YFP} were first incubated with anti-KDEL antibody after fixation and permeabilization of the cells, and subsequently, they were incubated with Alexa Fluor 546-conjugated anti-mouse IgG for anti-KDEL antibody. After treatments, fluorescent images of the cells derived from YFP (left panels) and Alexa Fluor 546 (middle panels) were obtained using a Bio-Rad MRC1024 laser scanning confocal microscopy. Right panels are merged images.

uptake into the cells expressing OCTN2VT and vector alone were 658 ± 9 and 603 ± 6 dpm/3 × 10⁵ cells, respectively ($n=3$, $P<0.05$) (Fig. 4A). The difference of these two values is a net uptake via OCTN2VT, which is about 0.20% of the uptake via OCTN2. After normalization of expression levels of OCTN2VT by MFI, the uptake by OCTN2VT is still far lower than the uptake by OCTN2. Considering that the MFI value obtained by FACS Calibur reflects expression levels of OCTN2VT in whole areas of individual cells but not on cell surface alone, and also that OCTN2VT is localized mainly in cytosol, the transport activity of each OCTN2VT molecule is estimated to be far higher than this estimated value. Since it is at present difficult to estimate the precise proportion of OCTN2VT expressed on the cell surface to total OCTN2VT expressed in the whole cell, the actual transport activity of each OCTN2VT molecule is unknown. Taken together, these results indicate that a minute amount of OCTN2VT with a carnitine transport activity is expressed, although it is unknown whether the activity of each OCTN2VT molecule is normal or reduced in comparison with that of wild type OCTN2.

To examine the relationship among N-glycosylation, expression level, and transport activity of OCTN2, we also analyzed the carnitine transport activity of OCTN2(N91Q): its expression level was about half of OCTN2 (Fig. 2F and G) and most of it was present on the cell surface (Fig. 4A, inset). The carnitine uptake into the cells expressing OCTN2(N91Q) was about half of OCTN2 (Fig. 4A). However, after normalization of its expression level by MFI, the transport activity was found to be not significantly different from the cells expressing OCTN2 (OCTN2(N91Q), $33.6 \pm 2.1 \times 10^3$ dpm/3 × 10⁵ cells; OCTN2, $26.7 \pm 1.3 \times 10^3$ dpm/3 × 10⁵ cells: $P>0.05$). These results imply that the reduction of glycosylation affects the expression level but not the transport activity of OCTN2.

A variety of mutations for OCTN2 have been reported in the systemic carnitine deficiency (SCD) of humans [5,17–20]. The Phe-17 to Leu mutation of OCTN2 identified in the SCD patient showed a reduction of V_{max} with no effect on K_m for carnitine transport due to its failure to be expressed on the cell surface [21]. Furthermore, Amat di San Filippo et al. have studied eight
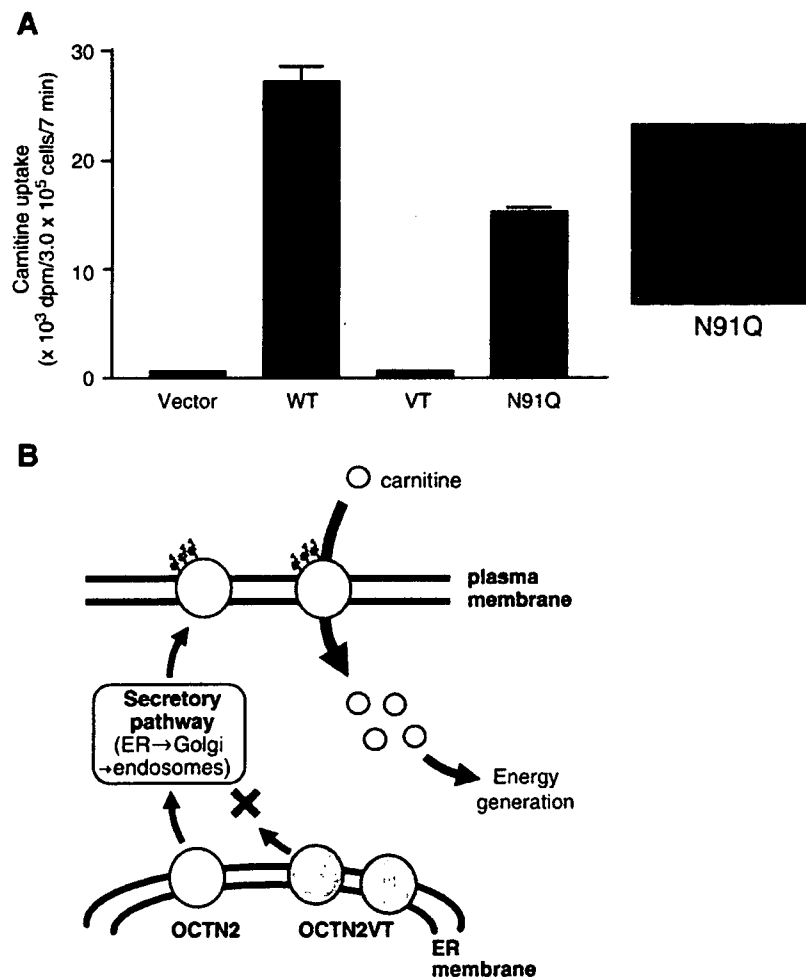

Fig. 4. Carnitine transport activity of OCTN2[YFP], OCTN2VT[YFP], and OCTN2(N91Q)[YFP]. (A) HeLa cells stably transfected with expression vectors containing cDNAs for either YFP (vector), OCTN2[YFP], OCTN2VT[YFP], and OCTN2(N91Q)[YFP] were incubated with a saturating concentration (4 nM) of [³H]carnitine (81 Ci/mmol) for 7 min at 37 °C. [³H]carnitine uptake into these cells were shown as mean±SEM ($n=3$). Inset: the subcellular distribution of OCTN2(N91Q)[YFP]. (B) Summary of the present study.

families with SCD and found several point mutations at sites other than glycosylation sites, which caused significant retention of the mutant OCTN2 in the cytoplasm [22]. Our results and these reports suggest that the subcellular localization of the OCTN family proteins is a critical factor for the pathogenesis of SCD.

Although it is not clear whether OCTN2VT transports carnitine if expressed on the plasma membrane, its actual function might transport organic cations across the ER membrane. It would provide new insights into the physiological functions of the OCTN family proteins to identify the substrate molecules transported by OCTN2VT.

3.5. Concluding remarks

Although the OCTN family proteins have been thought to be well conserved with respect to the biochemical and functional characteristics, the OCTN2VT protein isolated in this study showed unique characteristics, which are totally distinct from the OCTN2 and other OCTN family proteins. Our results demonstrate that OCTN2VT did not have the typical characteristics of OCTN family proteins, such as an N-glycosylation and cell surface expression, due to the insertion of 24 amino acids in the first extracellular loop of OCTN2. Furthermore, the HeLa cells expressing OCTN2VT proteins could not take up carnitine due to the retention of OCTN2VT proteins in the ER. The insertion of 24 amino acids may be made by the alternative splicing because the DNA sequence encoding the 24 amino acids was interposed between the conserved splice sites. Further investigation into the physiological functions of OCTN2VT in the ER may reveal the novel transport activity of OCTN family proteins across the ER membrane as well as the plasma membrane.

Acknowledgements

References

[1] K. Bartlett, S. Eaton, Mitochondrial beta-oxidation, Eur. J. Biochem. 271 (2004) 462–469.

[2] I. Tamai, R. Ohashi, J. Nezu, H. Yabuuchi, A. Oku, M. Shimane, Y. Sai, A. Tsuji, Molecular and functional identification of sodium ion-dependent, high affinity human carnitine transporter OCTN2, J. Biol. Chem. 273 (1998) 20378–20382.

[3] A.M. Lamhonwah, J. Skaug, S.W. Scherer, I. Tein, A third human carnitine/organic cation transporter (OCTN3) as a candidate for the 5q31 Crohn's disease locus (IBD5), Biochem. Biophys. Res. Commun. 301 (2003) 98–101.

[4] W. Xuan, A.M. Lamhonwah, C. Librach, K. Jarvi, I. Tein, Characterization of organic cation/carnitine transporter family in human sperm, Biochem. Biophys. Res. Commun. 306 (2003) 121–128.

[5] Y. Wang, J. Ye, V. Ganapathy, N. Longo, Mutations in the organic cation/carnitine transporter OCTN2 in primary carnitine deficiency, Proc. Natl. Acad. Sci. U. S. A. 96 (1999) 2356–2360.

[6] J. Nezu, I. Tamai, A. Oku, R. Ohashi, H. Yabuuchi, N. Hashimoto, H. Nikaido, Y. Sai, A. Koizumi, Y. Shoji, G. Takada, T. Matsuishi, M. Yoshino, H. Kato, T. Ohura, G. Tsujimoto, J. Hayakawa, M. Shimane, A. Tsuji, Primary systemic carnitine deficiency is caused by mutations in a gene encoding sodium ion-dependent carnitine transporter, Nat. Genet. 21 (1999) 91–94.

[7] R. Ohashi, I. Tamai, J. Nezu Ji, H. Nikaido, N. Hashimoto, A. Oku, Y. Sai, M. Shimane, A. Tsuji, Molecular and physiological evidence for multi-functionality of carnitine/organic cation transporter OCTN2, Mol. Pharmacol. 59 (2001) 358–366.

[8] I. Tamai, R. Ohashi, J.I. Nezu, Y. Sai, D. Kobayashi, A. Oku, M. Shimane, A. Tsuji, Molecular and functional characterization of organic cation/carnitine transporter family in mice, J. Biol. Chem. 275 (2000) 40064–40072.

[9] K. Nagai, O. Takikawa, N. Kawakami, M. Fukao, T. Soma, A. Oda, T. Nishiya, M. Hayashi, L. Lu, M. Nakano, E. Kajita, H. Fujita, S. Miwa, Cloning and functional characterization of a novel up-regulator, cartregulin, of carnitine transporter, OCTN2, Arch. Biochem. Biophys. 452 (2006) 29–37.

[10] T. Nishiya, E. Kajita, S. Miwa, A.L. Defranco, TLR3 and TLR7 are targeted to the same intracellular compartments by distinct regulatory elements, J. Biol. Chem. 280 (2005) 37107–37117.

[11] T. Nishiya, A.L. DeFranco, Ligand-regulated chimeric receptor approach reveals distinctive subcellular localization and signaling properties of the Toll-like receptors, J. Biol. Chem. 279 (2004) 19008–19017.

[12] T. Nishiya, T. Uehara, H. Edamatsu, Y. Kaziro, H. Itoh, Y. Nomura, Activation of Stat1 and subsequent transcription of inducible nitric oxide synthase gene in C6 glioma cells is independent of interferon-gamma-induced MAPK activation that is mediated by p21ras, FEBS Lett. 408 (1997) 33–38.

[13] G. Takaesu, S. Kishida, A. Hiyama, K. Yamaguchi, H. Shibuya, K. Irie, J. Ninomiya-Tsuji, K. Matsumoto, TAB2, a novel adaptor protein, mediates activation of TAK1 MAPKKK by linking TAK1 to TRAF6 in the IL-1 signal transduction pathway, Mol. Cell 5 (2000) 649–658.

[14] R.A. Padgett, P.J. Grabowski, M.M. Konarska, S. Seiler, P.A. Sharp, Splicing of messenger RNA precursors, Ann. Rev. Biochem. 55 (1986) 1119–1150.

[15] A. Helenius, M. Aebi, Intracellular functions of N-linked glycans, Science 291 (2001) 2364–2369.

[16] G. Chen, O. Frohlich, Y. Yang, J.D. Klein, J.M. Sands, Loss of N-linked glycosylation reduces urea transporter UT-A1 response to vasopressin, J. Biol. Chem. 281 (2006) 27436–27442.

[17] K. Lahjouji, G.A. Mitchell, I.A. Qureshi, Carnitine transport by organic cation transporters and systemic carnitine deficiency, Mol. Genet. Metab. 73 (2001) 287–297.

[18] C. Amat di San Filippo, N. Longo, Tyrosine residues affecting sodium stimulation of carnitine transport in the OCTN2 carnitine/organic cation transporter, J. Biol. Chem. 279 (2004) 7247–7253.

[19] Y. Wang, T.A. Meadows, N. Longo, Abnormal sodium stimulation of carnitine transport in primary carnitine deficiency, J. Biol. Chem. 275 (2000) 20782–20786.

[20] P. Seth, X. Wu, W. Huang, F.H. Leibach, V. Ganapathy, Mutations in novel organic cation transporter (OCTN2), an organic cation/carnitine transporter, with differential effects on the organic cation transport function and the carnitine transport function, J. Biol. Chem. 274 (1999) 33388–33392.

[21] T.J. Urban, R.C. Gallagher, C. Brown, R.A. Castro, L.L. Lagpacan, C.M. Brett, T.R. Taylor, E.J. Carlson, T.E. Ferrin, E.G. Burchard, S. Packman, K.M. Giacomini, Functional genetic diversity in the high-affinity carnitine transporter OCTN2 (SLC22A5), Mol. Pharmacol. 70 (2006) 1602–1611.

[22] C. Amat di San Filippo, M. Pasquali, N. Longo, Pharmacological rescue of carnitine transport in primary carnitine deficiency, Human Mutat. 27 (2006) 513–523.

Endothelin-1 decreases $[Ca^{2+}]_i$ via Na^+/Ca^{2+} exchanger in CHO cells stably expressing endothelin ET_A receptor

Takahiro Horinouchi, Arata Nishimoto, Tadashi Nishiya, Lingyun Lu, Emi Kajita, Soichi Miwa *

Department of Cellular Pharmacology, Hokkaido University Graduate School of Medicine, Sapporo 060-8638, Japan

Abstract

Endothelin ET_A receptor couples to $G_{q/11}$ protein that transduces a variety of receptor signals to modulate diverse cellular responses including Ca^{2+} mobilization. Stimulation of endothelin ET_A receptor with endothelin-1 is generally believed to induce an increase in intracellular Ca^{2+} concentration ($[Ca^{2+}]_i$) via $G_{q/11}$ protein. Here we provide the first convincing evidence that endothelin-1 elicited $G_{q/11}$ protein-dependent and -independent 'decrease' in $[Ca^{2+}]_i$ via Na^+/Ca^{2+} exchanger (NCX) in Chinese hamster ovary (CHO) cells stably expressing human endothelin ET_A receptor. In the cells treated with 1 μM thapsigargin, an inhibitor of endoplasmic Ca^{2+} pump, that induces an increase in $[Ca^{2+}]_i$ via capacitative Ca^{2+} entry, endothelin-1 induced a decrease in $[Ca^{2+}]_i$ which was partially inhibited by YM-254890, a specific inhibitor of $G_{q/11}$, indicating that $G_{q/11}$-dependent and independent pathways are involved in the decrease. The endothelin-1-induced decrease in $[Ca^{2+}]_i$ was markedly suppressed by 3′,4′-dichlorobenzamil hydrochloride, a potent NCX inhibitor, and also by a replacement of extracellular Na^+ with Li^+, which was not transported by NCX, indicating a major role of NCX operating in the forward mode in the endothelin-1-induced decrease in $[Ca^{2+}]_i$. Molecular approach with RT-PCR demonstrated the expression of mRNA for NCX1, NCX2 and NCX3. These results suggest that stimulation of endothelin ET_A receptor with endothelin-1 activates the forward mode NCX through $G_{q/11}$-dependent and -independent mechanisms: the NCX exports Ca^{2+} out of the cell depending on Na^+ gradient across the cell membrane, resulting in the decrease in $[Ca^{2+}]_i$.
© 2007 Elsevier B.V. All rights reserved.

1. Introduction

Endothelin ET_A receptor is a well studied member of the seven membrane spanning receptors that exert their intracellular effects through G protein activation (Kawanabe et al., 2002a,b; Miwa et al., 2005). Stimulation of endothelin ET_A receptor with endothelin-1 leads to $G_{q/11}$ protein-mediated activation of phospholipase C (PLC), resulting in the production of inositol 1,4,5-trisphosphate (IP_3) that binds to the IP_3 receptor in the endoplasmic reticulum (ER) membrane to initiate Ca^{2+} release into the cytosol (Kawanabe et al., 2002a; Miwa et al., 2005). This signal transduction pathway is associated with diverse subcellular mechanisms underlying an increase in intracellular free Ca^{2+} concentration ($[Ca^{2+}]_i$) induced by endothelin-1 such as activation of Ca^{2+}-permeable nonselective cation channel and store-operated Ca^{2+} channel (Miwa et al., 2005).

Recently, several studies demonstrated that endothelin-1 activated Na^+/H^+ exchanger (NHE), which increases intracellular Na^+ concentration ($[Na^+]_i$), leading to activation of Na^+/Ca^{2+} exchanger (NCX) operating in the reverse mode to increase $[Ca^{2+}]_i$ (Aiello et al., 2005; Fujita and Endoh, 1999; Yang et al., 1999). In addition, it has been reported that, after endothelin-1 stimulation, the NCX protein was phosphorylated by protein kinase C (PKC) which is a downstream signaling molecule activated by endothelin ET_A receptor (Iwamoto et al., 1996). A study with whole-cell patch clamp technique also showed that endothelin-1 induced a direct PKC-dependent increase in NCX-mediated outward ionic current which is reverse mode Na^+/Ca^{2+} exchange (Zhang et al., 2001). These results suggested that endothelin-1 induced Ca^{2+} influx is mediated by both mechanisms, the increase in $[Na^+]_i$ via NHE, which drives the NCX in the reverse mode, and a direct $[Na^+]_i$-independent activation of the NCX.

The NCX plays an important physiological role in maintaining Ca^{2+} homeostasis in many mammalian tissues (for review see, Blaustein and Lederer, 1999). The NCX can trigger the

* Corresponding author. Tel.: +81 11 706 6921; fax: +81 11 706 7824.
E-mail address: smiwa@med.hokudai.ac.jp (S. Miwa).

electrogenic exchange of one Ca^{2+} for three Na^+ either into or out of the cells, depending on the prevailing electrochemical driving force on the exchanger. In other words, excessive increase in $[Ca^{2+}]_i$ can lead to activation of NCX operating in the forward mode to transport Ca^{2+} out of cells. Therefore, we hypothesized that under high $[Ca^{2+}]_i$ conditions, endothelin-1 induces the decrease but not increase in $[Ca^{2+}]_i$ via the forward mode NCX driven by endothelin ET_A receptor activation, if endothelin-1 could directly activate NCX as described above.

To test this hypothesis, the present study examined the effects of endothelin-1 on the increase in $[Ca^{2+}]_i$ generated by thapsigargin, a sarcoplasmic and endoplasmic Ca^{2+}-ATPase inhibitor, in Chinese hamster ovary (CHO) cells stably expressing human endothelin ET_A receptor. The mechanisms underlying the Ca^{2+} mobilization activated by endothelin-1 were also studied using YM-254890, a novel and specific $G_{q/11}$ protein inhibitor (Takasaki et al., 2004; Taniguchi et al., 2003), and $3',4'$-dichlorobenzamil hydrochloride ($3',4'$-DCB), a potent forward and reverse mode NCX inhibitor (Teubl et al., 1999).

2. Materials and methods

2.1. Materials

YM-254890 (Fig. 1, molecular weight=959, Taniguchi et al., 2003) was kindly provided by the Astellas Pharma Inc. (Tokyo, Japan). Other chemicals were obtained commercially from the following sources: synthetic human endothelin-1 from Peptide Institute (Osaka, Japan); $3',4'$-dichlorobenzamil hydrochloride ($3',4'$-DCB), probenecid and thapsigargin from Sigma-Aldrich Co. (St. Louis, Mo., U.S.A.); U-73122 (1-[6-((17β-3-methox-yestra-1,3,5(10)-trien-17-yl)amino)hexyl]-1H-pyrrole-2,5-dione) from Calbiochem (San Diego, CA, U.S.A.); fura-2/acetoxymethyl ester (fura-2/AM), fluo-3/acetoxymethyl ester (fluo-3/AM) and Pluronic F-127 from Dojindo Laboratories (Kumamoto, Japan).

2.2. Cell culture

CHO cells were cultured in Ham's F-12 medium supplemented with 10% fetal calf serum and penicillin–streptomycin at 37 °C in humidified air with 5% CO_2.
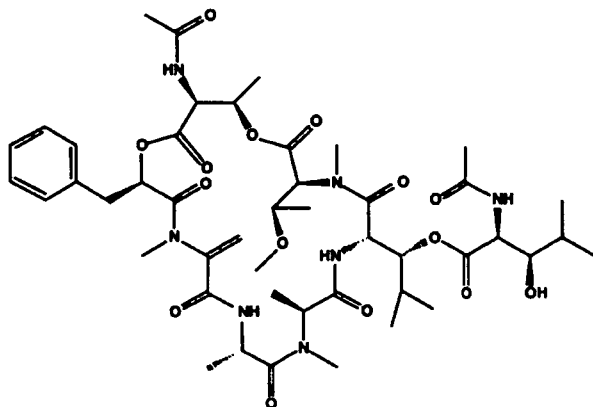

Fig. 1. Chemical structure of YM-254890.

2.3. Stable expression of human endothelin ET_A receptor in CHO cells

To generate CHO cells stably expressing endothelin ET_A receptor, human endothelin ET_A receptor gene was introduced into CHO cells by retroviral gene transfer. Briefly, retroviruses were produced by triple transfection of HEK293T cells with retroviral constructs along with gag-pol and vesicular stomatitis virus G glycoprotein expression constructs (Yee et al., 1994). The supernatants containing virus were collected 24 h after transfection and added to CHO cells. The CHO cells were then centrifuged at 900 ×g for 45 min at room temperature followed by incubation for 6 h at 37 °C in 5% CO_2–95% air. Then, the supernatants were replaced with fresh culture media. Endothelin ET_A receptor-positive cells were selected for growth in medium containing 5 µg/ml puromycin for a week.

2.4. Measurement of $[Ca^{2+}]_i$

CHO cells grown to confluence in 10-cm dishes were incubated in the culture medium with 4 µM fura-2/AM or 10 µM fluo-3/AM admixed with 2.5 mM probenecid and 0.04% Pluronic F-127, a detergent, at 37 °C for 45 min under reduced light. Cells were then collected and washed once with Ca^{2+}-free Krebs-HEPES solution (in mM: 140 NaCl, 3 KCl, 1 $MgCl_2\cdot6H_2O$, 11 D-(+)-glucose, 10 HEPES; adjusted to pH 7.3 with LiOH). The resulting cell pellets were resuspended in Ca^{2+}-free Krebs-HEPES solution at 4×10^5 cells/ml and kept on ice under reduced light until Ca^{2+} measurement.

In some experiments, cells were resuspended in low Na^+ Krebs-HEPES solutions (0, 10 and 70 mM Na^+) prepared by replacing NaCl with equimolar LiCl. Before each experiment, $CaCl_2$ was added to 0.5-ml aliquot of the cell suspension at the final concentration of 1 mM.

Changes of $[Ca^{2+}]_i$ in cells were measured at 25 °C using CAF-110 spectrophotometer (JASCO, Tokyo, Japan) with the following wavelengths: fura-2 excitation=340 and 380 nm, emission=500 nm; fluo-3 excitation=490 nm, emission=540 nm. At the end of each experiment, Triton X-100 was added to the cells at the final concentration of 0.2% to determine the maximal fluorescence intensity (F_{max}) and/or ratio ($R340/380_{max}$). This was followed by an addition of EGTA at the final concentration of 30 mM to determine the minimal fluorescence intensity (F_{min}) and/or ratio ($R340/380_{min}$). $[Ca^{2+}]_i$ was calculated as previously described (Grynkiewicz et al., 1985; Minta et al., 1989).

In the experiments with $3',4'$-DCB, $[Ca^{2+}]_i$ was measured using fluo-3 instead of fura-2, because $3',4'$-DCB over 10 µM used in the present study was found to interfere with fluorescence signals of fura-2 (data not shown).

2.5. Detection of mRNA by reverse transcription-polymerase chain reaction (RT-PCR)

mRNA was extracted and purified using the mRNA purification kit (GE Healthcare UK Ltd., Buckinghamshire, UK) following the instructions of the manufacturer. cDNA was synthesized by using both Omniscript™ RT Kit (QIAGEN,

Tokyo, Japan) for reverse transcription (RT) and HotStarTaq™ Master Mix Kit (QIAGEN, Tokyo, Japan) for polymerase chain reaction (PCR). Briefly, cDNA was synthesized by RT of 2.0 μg of each mRNA using oligo (dT)$_{15}$ (Promega, Madison, U.S.A.) as a primer, and the RT reaction mixture was incubated at 37 °C for 60 min, then at 95 °C for 5 min before being placed on ice. A negative control without reverse transcriptase was run in parallel to verify that amplification did not proceed from residual genomic DNA.

PCR amplification was carried out on cDNA equivalent to 100 ng of starting mRNA, using specific oligonucleotide primers for NCX1 (forward, 5′-AATGGAGAGACCACCAAGAC-3′ and reverse, 5′-CCTTCCCAGACCTCCAC-3′), NCX2 (forward, 5′-GAGATCACCATCACCAAGGC-3′ and reverse, 5′-ATGA-GATAAAGCCAGACATAGGC-3′) and NCX3 (forward, 5′-TCTCACCTCTGCCTTCCTCCATTT-3′ and reverse, 5′-TCAGGTTGGAGACAGTTTCATTCCA-3′), synthesized at Hokkaido System Science Co., Ltd. (Sapporo, Japan). cDNA was heated for 15 min at 95 °C, then amplified by 35 cycles (95 °C for 30 s, 55 °C for 30 s, 72 °C for 30 s) followed by 5 min of extension at 72 °C. The PCR products were confirmed by a single band on electrophoresis with 2.0% ethidium bromide stained agarose gels. Because the sequences for NCX1, NCX2 and NCX3 of Chinese hamster were unknown, the primer sets were designed using conserved sequences for NCX mRNA among human, rat and mouse. To confirm the sequences of these PCR products, the direct sequencing was carried out. Briefly, the PCR products of NCX1, NCX2 and NCX3 were purified using QIAquick™ PCR Purification Kit (QIAGEN, Tokyo, Japan) according to the manufacturer's instructions. The purified PCR products were labeled using BigDye™ Terminator v3.1 Cycle Sequencing Kit (Applied Biosystem, CA, U.S.A.) and the aforementioned primers. DNA sequencing was performed on the ABI PRISM™3100 Genetic Analyzer (Applied Biosystem, CA, U.S.A.).

2.6. Data analysis

The percentage of decrease in [Ca^{2+}]$_i$ induced by endothelin-1 was calculated by considering the [Ca^{2+}]$_i$ level obtained just before administration of endothelin-1 as 0% decrease, and the basal [Ca^{2+}]$_i$ level before application of thapsigargin as 100% decrease. Data are presented as means±S.E.M. where n refers to the number of experiments. The significance of the difference between mean values was evaluated with GraphPad PRISM™ (version 3.00) by one-way analysis of variance (ANOVA) followed by Tukey's multiple comparison test. A P value less than 0.05 was considered to indicate significant differences.

3. Results

3.1. Dual effects of endothelin-1 in the regulation of [Ca^{2+}]$_i$

Figs. 2A and 3A show representative traces for the opposite effects of 0.3 nM endothelin-1 on [Ca^{2+}]$_i$ in CHO cells stably expressing endothelin ET$_A$ receptor. In untreated cells, endothelin-1 induced transient and subsequent sustained increases in [Ca^{2+}]$_i$ (Fig. 2A, left trace), which were
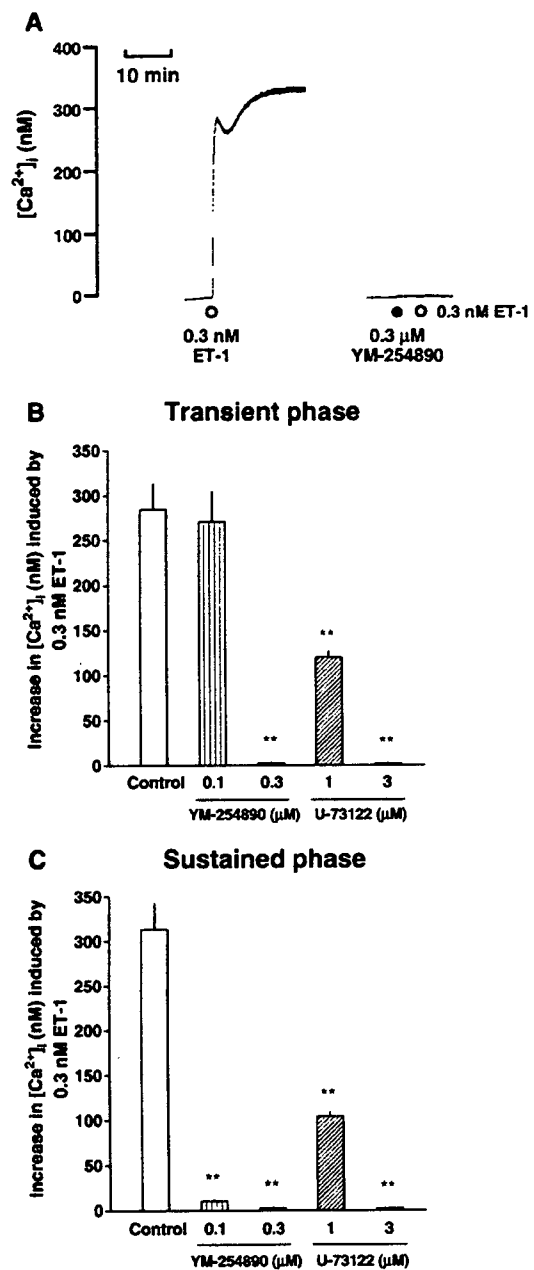

Fig. 2. Characterization of endothelin-1-induced increase in intracellular free Ca^{2+} concentration ([Ca^{2+}]$_i$) in CHO cells stably expressing human endothelin ET$_A$ receptor. (A) Endothelin-1 induced transient and sustained increases in [Ca^{2+}]$_i$ (left trace). Both phases were completely abolished by YM-254890 (0.3 μM), a specific G$_{q/11}$ protein inhibitor (right trace). The traces shown are representative of 5 similar individual experiments. (B and C) Effects of YM-254890 and U-73122, a PLC inhibitor, on the transient and sustained increases in [Ca^{2+}]$_i$ induced by endothelin-1. The transient and sustained [Ca^{2+}]$_i$ increases were inhibited by the pretreatment with YM-254890 and U-73122. Thus the Ca^{2+} responses to endothelin-1 are mediated by G$_{q/11}$/PLC pathway. The ordinate is the change in [Ca^{2+}]$_i$ measured using a Ca^{2+} indicator fura-2. Results are presented as means±S.E.M of the results obtained from 4–6 separate experiments. **$P<0.01$.

submaximal responses. Both phases were completely abolished by pretreatment with 0.3 μM YM-254890, a specific and potent G$_{q/11}$ protein inhibitor (Fig. 2A, right trace). In addition, U-73122, an inhibitor of PLC, at a concentration of 3 μM
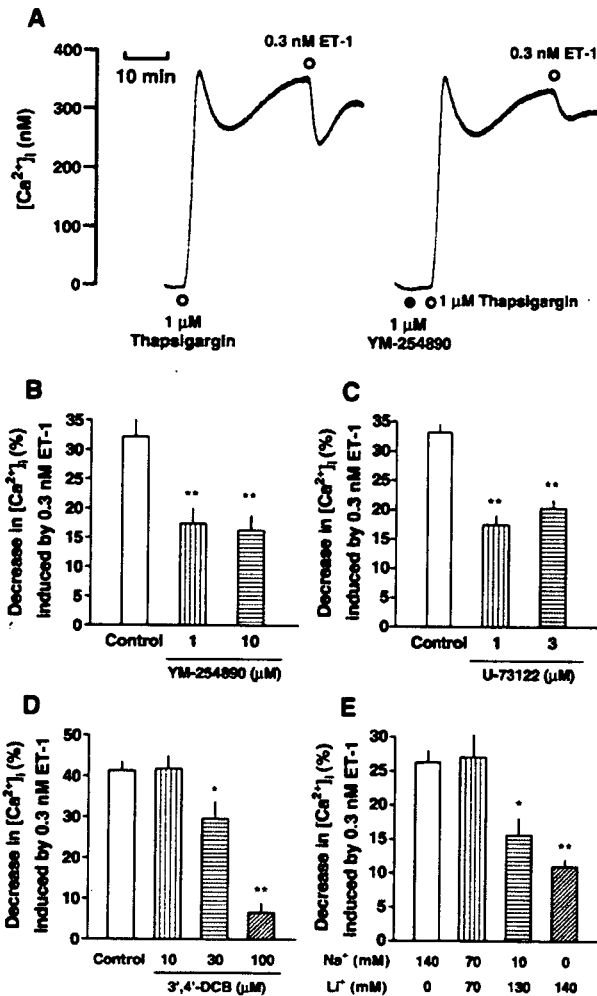
A

B

C

D

E

Fig. 3. Endothelin-1 can induce a decrease in $[Ca^{2+}]_i$ in CHO cells stably expressing human endothelin ET_A receptor. (A) Thapsigargin (1 μM) also evoked transient and sustained increases in $[Ca^{2+}]_i$. Stimulation of ET_A receptors with endothelin-1 inhibited the sustained phase generated by thapsigargin (left trace). Endothelin-1-induced decrease in $[Ca^{2+}]_i$ was partly inhibited by the pretreatment with the high concentration (1 μM) of YM-254890 (right trace). The ordinate is the change in $[Ca^{2+}]_i$ measured using a Ca^{2+} indicator fura-2. The traces shown are representative of 5 similar individual experiments. (B and C) YM-254890 and U-73122 could partially inhibit endothelin-1-induced decrease in $[Ca^{2+}]_i$. Thus the Ca^{2+} response to endothelin-1 is mediated by $G_{q/11}$/PLC-dependent and -independent pathways. (D) 3′,4′-DCB. a potent Na^+/Ca^{2+} exchanger inhibitor, significantly suppressed endothelin-1-induced decrease in $[Ca^{2+}]_i$. (E) A reduction of extracellular Na^+ concentration by replacement of Na^+ with Li^+ in bathing medium resulted in marked inhibition of endothelin-1-induced decrease in $[Ca^{2+}]_i$. The $[Ca^{2+}]_i$ level of sustained phase generated by thapsigargin before administration of endothelin-1 and the basal $[Ca^{2+}]_i$ level before administration of thapsigargin were set at 0% and 100%, respectively. Results are presented as means±S.E.M of the results obtained from 4–6 separate experiments. $*P<0.05$, $**P<0.01$.

depressed the transient and sustained $[Ca^{2+}]_i$ increases in response to 0.3 nM endothelin-1 (Fig. 2B, C). The result is in accord with our previous report (Sugawara et al., 1996). As shown in Fig. 3A, the treatment of CHO cells with 1 μM thapsigargin, a sarcoplasmic and endoplasmic Ca^{2+}-ATPase inhibitor, elicited transient and sustained increases in $[Ca^{2+}]_i$. Surprisingly, endothelin-1 at 0.3 nM caused a significant

reduction of $[Ca^{2+}]_i$ (32.2±2.8% of thapsigargin-induced sustained increase in $[Ca^{2+}]_i$, $n=5$; Fig. 3B), after the sustained increase in $[Ca^{2+}]_i$ induced by thapsigargin reached a plateau level (Fig. 3A, left trace). The decrease in $[Ca^{2+}]_i$ induced by endothelin-1 was partly but significantly inhibited by 1 μM YM-254890 (17.4±2.6%, $n=5$; Fig. 3B). However, a higher concentration (10 μM) of YM-254890 did not show further inhibition of $[Ca^{2+}]_i$ reduction (16.2±2.5%, $n=5$; Fig. 3B), indicating that the inhibitory effect of YM-254890 was maximal at 1 μM. Similarly, U-73122 inhibited the endothelin-1-induced $[Ca^{2+}]_i$ decrease (Fig. 3C). These results suggested that the decrease in $[Ca^{2+}]_i$ induced by endothelin-1 was mediated through $G_{q/11}$-dependent and -independent pathways.

3.2. Functional role of NCX in the decrease in $[Ca^{2+}]_i$ induced by endothelin-1

To clarify the mechanisms involving the decrease in $[Ca^{2+}]_i$ induced by endothelin-1, the effects of 3′,4′-dichlorobenzamil hydrochloride (3′,4′-DCB), a forward and reverse mode NCX inhibitor (Teubl et al., 1999), were investigated using a Ca^{2+} indicator fluo-3 instead of fura-2 (see Materials and methods). As shown in Fig. 3D, 3′,4′-DCB at concentrations over 30 μM depressed the decrease in $[Ca^{2+}]_i$ induced by endothelin-1 in a concentration-dependent manner (control, 41.3±2.3%; 10 μM 3′,4′-DCB, 41.8±3.0%; 30 μM, 29.6±4.1%; 100 μM, 6.5± 2.2%; $n=5$ for each).

In addition, the YM-254890-insensitive ($G_{q/11}$-independent) decrease was markedly inhibited by 100 μM 3′,4′-DCB (in the presence of 1 μM YM-254890, 23.2±0.9%; the combination of 1 μM YM-254890 and 100 μM 3′,4′-DCB, 2.4±0.6%; $n=6$). These results indicate that the forward mode NCX transporting Ca^{2+} out of cells plays an important role in both $G_{q/11}$-dependent and -independent decreases in $[Ca^{2+}]_i$ triggered by endothelin-1.

To further confirm the possible involvement of NCX operating in the forward mode, where its driving force is generated by the concentration gradient of Na^+ across the membrane, we attempted to examine the decreasing concentrations of extracellular Na^+ on the activity of NCX associated with the endothelin-1-induced decrease in $[Ca^{2+}]_i$.

For this purpose, we reduced the extracellular Na^+ concentration by replacing Na^+ with Li^+, which was not transported by NCX (Blaustein and Lederer, 1999). As expected, the endothelin-1-induced decrease in $[Ca^{2+}]_i$ became smaller depending on the decreasing concentrations of extracellular Na^+ (Fig. 3E). Taken together, these results suggest that stimulation of endothelin ET_A receptor with endothelin-1 activates the forward mode NCX to drive Ca^{2+} efflux and Na^+ influx in $G_{q/11}$-dependent and -independent manner, resulting in the decrease in $[Ca^{2+}]_i$.

3.3. Expression of mRNA for NCX1, NCX2 and NCX3 in CHO cells

To validate the pharmacological and physiological evidence for the presence of functional NCX in CHO cells stably expressing endothelin ET_A receptor, RT-PCR experiments were carried out. As shown in Fig. 4, PCR products were detected by
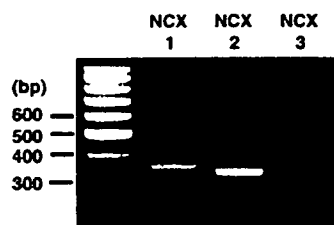
Fig. 4. Detection by RT-PCR of NCX1, NCX2 and NCX3 mRNA in CHO cells stably expressing human endothelin ET$_A$ receptor. RT-PCR experiments were carried out using mRNA prepared from 3 individual cell populations. Expected size of PCR products for NCX1, NCX2 and NCX3 were 350, 329 and 386 bp, respectively. Left lane shows 100 bp DNA ladder (Promega).

agarose gel electrophoresis at positions of approximately 350, 330 and 390 bp, which correspond to the expected size for PCR products of NCX1 (350 bp), NCX2 (329 bp) and NCX3 (386 bp), respectively. The absence of PCR products without reverse transcription provided evidence that there is no non-specific amplification and these bands are derived from mRNA but not contaminating genomic DNA (data not shown). Finally, the PCR products were purified, sequenced and identified as NCX1, NCX2 and NCX3. The degree of sequence homology for NCX1, NCX2 and NCX3 between Chinese hamster and the three species (human, rat and mouse) was approximately 90%.

4. Discussion

In the present study, we have provided the first evidence that stimulation of endothelin ET$_A$ receptor with endothelin-1 induces G$_{q/11}$ protein-dependent and -independent decreases in [Ca^{2+}]$_i$ via NCX operating in the forward mode in CHO cells stably expressing human endothelin ET$_A$ receptor. In addition, we were able to detect all three types of NCX (NCX1, NCX2 and NCX3) by using RT-PCR.

4.1. Involvement of G$_{q/11}$ protein-dependent and -independent pathways in endothelin ET$_A$ receptor signaling

To characterize endothelin ET$_A$ receptor signaling, we examined the effects of YM-254890, a novel and specific G$_{q/11}$ protein inhibitor, on endothelin-1-mediated Ca^{2+} mobilization. Initial studies confirmed that YM-254890 blocked Ca^{2+} mobilization mediated by several G$_{q/11}$-coupled receptors but not by G$_i$- or G$_{\alpha 15}$-coupled receptors (Takasaki et al., 2004). In the present study, in CHO cells expressing human endothelin ET$_A$ receptor, YM-254890 (0.3 μM) completely inhibited endothelin-1-induced transient and sustained increases in [Ca^{2+}]$_i$ (Fig. 2A). Similar results were obtained for a PLC inhibitor, U-73122. These results indicate the activation of G$_{q/11}$ and its downstream signaling pathways by endothelin-1.

Interestingly, in CHO cells pretreated with thapsigargin which induces an increase in [Ca^{2+}]$_i$ mediated by capacitative Ca^{2+} entry, endothelin-1 induced a marked decrease in [Ca^{2+}]$_i$, as shown in Fig. 3A. The decrease consisted of two components, which were sensitive and insensitive to YM-254890 at pharmacologically relevant concentrations. This result indicates that the

endothelin-1-induced decrease in [Ca^{2+}]$_i$ is mediated via both G$_{q/11}$-dependent and -independent pathways. We have recently shown that endothelin ET$_A$ receptor is functionally coupled with G$_s$ and G$_{12}$ in addition to G$_{q/11}$ in CHO cells (Kawanabe et al., 2002a; Takagi et al., 1995). G$_s$ protein is a possible candidate for G$_{q/11}$-independent mechanisms involving the endothelin-1-induced [Ca^{2+}]$_i$ decrease, because the activation of β-adrenoceptors, a member of G$_s$ protein-coupled receptors, is reported to induce the reduction of [Ca^{2+}]$_i$ via NCX in the porcine coronary arterial smooth muscle (Yamanaka et al., 2003). However, G$_s$-adenylyl cyclase pathway(s) might be ruled out, since an inhibitor of adenylyl cyclase (2′,5′-dideoxyadenosine, 50 μM) had no effect on the endothelin-1-induced decrease in [Ca^{2+}]$_i$ (data not shown). Therefore, G$_{12}$ and/or other unidentified G protein(s) may be responsible for G$_{q/11}$-independent pathway(s).

4.2. Identification of molecules involved in the endothelin-1-induced decrease in [Ca^{2+}]$_i$

Although the mechanisms for endothelin-1-induced increase in [Ca^{2+}]$_i$ have so far been reported repeatedly, there was no report for the endothelin-1-induced decrease in [Ca^{2+}]$_i$. We therefore attempted to clarify possible mechanisms underlying this response. For this purpose, we focused on the physiological role of NCX that can transport Ca^{2+} either into or out of cells depending on transmembrane ion gradient and membrane potential, since stimulation of G$_{q/11}$ protein-coupled receptors with endothelin-1, phenylephrine and angiotensin II activated cardiac NCX operating in the forward mode (Ballard and Schaffer, 1996; Philipson and Nicoll, 2000). Endothelin-1-induced decrease in [Ca^{2+}]$_i$ was, as expected, significantly depressed by 3′,4′-DCB, a forward and reverse mode NCX inhibitor (Teubl et al., 1999), in a concentration-dependent manner. In addition, the response to endothelin-1 was also inhibited by the reduction of extracellular Na$^+$ concentration which is expected to decrease NCX driving force in the forward mode. These results strongly indicate that the forward mode NCX transporting Ca^{2+} out of cells plays a significant role in G$_{q/11}$-dependent and -independent Ca^{2+} export activated by endothelin-1. However, the removal of Na$^+$ from the medium to block ion transport via NCX did not completely prevent endothelin-1-induced decrease in [Ca^{2+}]$_i$. This raises the possibility that endothelin-1-induced [Ca^{2+}]$_i$ decrease is mediated through NCX-dependent and -independent pathways. Unlike the NCX-dependent pathway, the NCX-independent mechanism involving Ca^{2+} export is still unclear.

4.3. Molecular evidence for the presence of NCX in CHO cells

Previous molecular studies have identified NCX1, NCX2 and NCX3 that are encoded by distinct genes in mammalian cells (Li et al., 1994; Nicoll et al., 1990, 1996). To determine whether either the NCX member is present in CHO cells, we performed RT-PCR using specific primers for each of these NCX genes. The RT-PCR studies demonstrated that all three members of NCX were expressed in CHO cells stably expressing endothelin ET$_A$ receptor. That is, the sequence of PCR products was highly

homologous (approximately 90%) to that of the corresponding NCX member reported in human, rat and mouse, and hence, the mRNAs containing these sequences were identified as NCX1, NCX2 and NCX3. This is the first report of mRNA expression and function of NCX in CHO cells. However, it remains to be determined which of the NCX members plays a major role after stimulation of endothelin ET_A receptor, because NCX1, NCX2 and NCX3 cannot be functionally differentiated (Iwamoto and Shigekawa, 1998; Linck et al., 1998). Therefore, the pharmacological and molecular identity should be determined by using RNA interference method for specific NCX gene silencing in future. .

In summary, the present study demonstrated that the functionally tight coupling of endothelin ET_A receptor with NCX induced the decrease in $[Ca^{2+}]_i$ in CHO cells. This association would play a regulatory role in Ca^{2+} homeostasis.

Acknowledgements

References

Aiello, E.A., Villa-Abrille, M.C., Dulce, R.A., Cingolani, H.E., Perez, N.G., 2005. Endothelin-1 stimulates the Na^+/Ca^{2+} exchanger reverse mode through intracellular Na^1 (Na^1)-dependent and Na^1-independent pathways. Hypertension 45, 288–293.

Ballard, C., Schaffer, S., 1996. Stimulation of the Na^+/Ca^{2+} exchanger by phenylephrine, angiotensin II and endothelin 1. J. Mol. Cell. Cardiol. 28, 11–17.

Blaustein, M.P., Lederer, W.J., 1999. Sodium/calcium exchange: its physiological implications. Physiol. Rev. 79, 763–854.

Fujita, S., Endoh, M., 1999. Influence of a Na^+-H^+ exchange inhibitor ethylisopropylamiloride, a Na^1-Ca^{2+} exchange inhibitor KB-R7943 and their combination on the increases in contractility and Ca^{2-} transient induced by angiotensin II in isolated adult rabbit ventricular myocytes. Naunyn-Schmiedeberg's Arch. Pharmacol. 360, 575–584.

Grynkiewicz, G., Poenie, M., Tsien, R.Y., 1985. A new generation of Ca^{2+} indicators with greatly improved fluorescence properties. J. Biol. Chem. 260, 3440–3450.

Iwamoto, T., Shigekawa, M., 1998. Differential inhibition of Na^1/Ca^{2+} exchanger isoforms by divalent cations and isothiourea derivative. Am. J. Physiol. 275, C423–C430.

Iwamoto, T., Pan, Y., Wakabayashi, S., Imagawa, T., Yamanaka, H., Shigekawa, M., 1996. Phosphorylation-dependent regulation of cardiac Na^1/Ca^{2+} exchanger via protein kinase C. J. Biol. Chem. 271, 13609–13615.

Kawanabe, Y., Okamoto, Y., Miwa, S., Hashimoto, N., Masaki, T., 2002a. Molecular mechanisms for the activation of voltage-independent Ca^{2+} channels by endothelin-1 in Chinese hamster ovary cells stably expressing human endothelin$_A$ receptors. Mol. Pharmacol. 62, 75–80.

Kawanabe, Y., Okamoto, Y., Nozaki, K., Hashimoto, N., Miwa, S., Masaki, T., 2002b. Molecular mechanism for endothelin-1-induced stress-fiber formation: analysis of G proteins using a mutant endothelin$_A$ receptor. Mol. Pharmacol. 61, 277–284.

Li, Z., Matsuoka, S., Hryshko, L.V., Nicoll, D.A., Bersohn, M.M., Burke, E.P., Lifton, R.P., Philipson, K.D., 1994. Cloning of the NCX2 isoform of the plasma membrane Na^+-Ca^{2+} exchanger. J. Biol. Chem. 269, 17434–17439.

Linck, B., Qiu, Z., He, Z., Tong, Q., Hilgemann, D.W., Philipson, K.D., 1998. Functional comparison of the three isoforms of the Na^-/Ca^{2+} exchanger (NCX1, NCX2, NCX3). Am. J. Physiol. 274, C415–C423.

Minta, A., Kao, J.P.Y., Tsieng, R.Y., 1989. Fluorescent indicators for cytosolic calcium based on rhodamine and fluorescein chromophores. J. Biol. Chem. 264, 8171–8178.

Miwa, S., Kawanabe, Y., Okamoto, Y., Masaki, T., 2005. Ca^{2+} entry channels involved in endothelin-1-induced contractions of vascular smooth muscle cells. J. Smooth Muscle Res. 41, 61–75.

Nicoll, D.A., Longoni, S., Philipson, K.D., 1990. Molecular cloning and functional expression of the cardiac sarcolemmal Na^+-Ca^{2+} exchanger. Science 250, 562–565.

Nicoll, D.A., Quednau, B.D., Qui, Z., Xia, Y.R., Lusis, A.J., Philipson, K.D., 1996. Cloning of a third mammalian Na^-Ca^{2+} exchanger, NCX3. J. Biol. Chem. 271, 24914–24921.

Philipson, K.D., Nicoll, D.A., 2000. Sodium–calcium exchange: a molecular perspective. Annu. Rev. Physiol. 62, 111–113.

Sugawara, F., Ninomiya, H., Okamoto, Y., Miwa, S., Mazda, O., Katsura, Y., Masaki, T., 1996. Endothelin-1-induced mitogenic responses of Chinese hamster ovary cells expressing human endothelin$_A$: the role of a wortmannin-sensitive signaling pathway. Mol. Pharmacol. 49, 447–457.

Takagi, Y., Ninomiya, H., Sakamoto, A., Miwa, S., Masaki, T., 1995. Structural basis of G protein specificity of human endothelin receptors. A study with endothelin$_{A/B}$ chimeras. J. Biol. Chem. 270, 10072–10078.

Takasaki, J., Saito, T., Taniguchi, M., Kawasaki, T., Moritani, Y., Hayashi, K., Kobori, M., 2004. A novel $G_{\alpha q/11}$-selective inhibitor. J. Biol. Chem. 279, 47438–47445.

Taniguchi, M., Nagai, K., Arao, N., Kawasaki, T., Saito, T., Moritani, Y., Takasaki, J., Hayashi, K., Fujita, S., Suzuki, K., Tsukamoto, S., 2003. YM-254890, a novel platelet aggregation inhibitor produced by *Chromobacterium* sp. QS3666. J. Antibiot. 56, 358–363.

Teubl, M., Groschner, K., Kohlwein, S.D., Mayer, B., Schmidt, K., 1999. Na^+/Ca^{2+} exchange facilitates Ca^{2+}-dependent activation of endothelial nitric-oxide synthase. J. Biol. Chem. 274, 29529–29535.

Yamanaka, J., Nishimura, J., Hirano, K., Kanaide, H., 2003. An important role for the Na^+-Ca^{2+} exchanger in the decrease in cytosolic Ca^{2+} concentration induced by isoprenaline in the porcine coronary artery. J. Physiol. 549, 553–562.

Yang, H., Sakurai, K., Sugawara, H., Watanabe, T., Norota, I., Endoh, M., 1999. Role of Na^+/Ca^{2-} exchange in endothelin-1-induced increases in Ca^{2+} transient and contractility in rabbit ventricular myocytes: pharmacological analysis with KB-R7943. Br. J. Pharmacol. 126, 1785–1795.

Yee, J.K., Friedmann, T., Burns, J.C., 1994. Generation of high-titer pseudotyped retroviral vectors with very broad host range. Methods Cell Biol. 43, 99–112.

Zhang, Y.H., James, A.F., Hancox, J.C., 2001. Regulation by endothelin-1 of Na^+-Ca^{2+} exchange current (I_{NaCa}) from guinea-pig isolated ventricular myocytes. Cell Calcium 30, 351–360.

Full Paper

Characterization of Noradrenaline-Induced Increases in Intracellular Ca²⁺ Levels in Chinese Hamster Ovary Cells Stably Expressing Human α1A-Adrenoceptor

Takahiro Horinouchi[1], Yumie Miyake[1], Tadashi Nishiya[1], Arata Nishimoto[1], Shoko Yorozu[1], Atsushi Jinno[1], Emi Kajita[1], and Soichi Miwa[1,*]

[1]*Department of Cellular Pharmacology, Hokkaido University Graduate School of Medicine, Sapporo 060-8638, Japan*

Abstract. The mechanism for noradrenaline (NA)-induced increases in intracellular Ca^{2+} concentration ($[Ca^{2+}]_i$) and physiological significance of Na^+ influx through receptor-operated channels (ROCs) and store-operated channels (SOCs) were studied in Chinese hamster ovary (CHO) cells stably expressing human α1A-adrenoceptor (α1A-AR). $[Ca^{2+}]_i$ was measured using the Ca^{2+} indicator fura-2. NA (1 μM) elicited transient and subsequent sustained $[Ca^{2+}]_i$ increases, which were inhibited by YM-254890 ($G_{\alpha q/11}$ inhibitor), U-73122 (phospholipase C (PLC) inhibitor), and bisindolylmaleimide I (protein kinase C (PKC) inhibitor), suggesting their dependence on $G_{\alpha q/11}$/PLC/PKC. Both phases were suppressed by extracellular Ca^{2+} removal, SK&F 96365 (inhibitor of SOC and nonselective cation channel type-2 (NSCC-2)), LOE 908 (inhibitor of NSCC-1 and NSCC-2), and La^{3+} (inhibitor of transient receptor potential canonical (TRPC) channel). Reduction of extracellular Na^+ and pretreatment with KB-R7943, a Na^+/Ca^{2+} exchanger (NCX) inhibitor, inhibited both phases of $[Ca^{2+}]_i$ increases. These results suggest that 1) stimulation of α1A-AR with NA elicits the transient and sustained increases in $[Ca^{2+}]_i$ mediated through NSCC-2 that belongs to a TRPC family; 2) Na^+ influx through these channels drives NCX in the reverse mode, causing Ca^{2+} influx in exchange for Na^+ efflux; and 3) the $G_{\alpha q/11}$/PLC/PKC-dependent pathway plays an important role in the increases in $[Ca^{2+}]_i$.

Keywords: α1A-adrenoceptor, store-operated channel, nonselective cation channel, Na^+/Ca^{2+} exchanger, intracellular free Ca^{2+} concentration

Introduction

The α1A-adrenoceptor (α1A-AR) belongs to the superfamily of G protein-coupled receptors (GPCRs) that transduce the binding of their agonists such as the neurotransmitter noradrenaline (NA) into activation of G protein-regulated effectors and elevation of corresponding second messengers. In general, stimulation of α1A-ARs with NA activates $G_{q/11}$ protein-coupled phospholipase Cβ (PLCβ) to increase the second messengers, inositol 1,4,5-trisphosphate (IP₃) and diacylglycerol (DAG), thereby causing an initial transient increase and a subsequent sustained increase in $[Ca^{2+}]_i$ (1).

In most nonexcitable cells including Chinese hamster ovary (CHO) cells, this interdependent mobilization of Ca^{2+} is considered to be attributed to rapid, transient release of Ca^{2+} stored in the endoplasmic reticulum (ER), followed by slowly developing Ca^{2+} entry through store-operated channels (SOCs) and/or receptor-operated channels (ROCs) such as Ca^{2+}-permeable nonselective cation channels (NSCCs) (2 – 5). Our previous studies have demonstrated that NA-induced sustained Ca^{2+} influx through NSCCs plays an essential role in cell proliferation and arachidonic acid release following stimulation of α1A-AR expressed in CHO cells (1, 6). Interestingly, Mori and colleagues (7) have demonstrated that the essential component of NA-activated NSCC is the transient receptor potential canonical (TRPC) channel homologue TRPC6 since heterologous expression of murine TRPC6 in human embryonic

kidney (HEK293) cells reproduced the biophysical and pharmacological properties of NA-activated NSCC. These findings suggest that voltage-independent (non-voltage-gated) cation channels (SOCs, ROCs, NSCCs, and TRPC channels) are involved in NA-induced Ca^{2+} influx.

Ca^{2+} signal plays a key role in controlling diverse cellular functions such as contraction, proliferation, and transcription (8). GPCR mediating Ca^{2+} influx across the plasma membrane, therefore, is strictly regulated by complicated mechanisms involving cation channels such as SOCs and ROCs (2, 9). On the other hand, many studies have shown that most of these channels allow the entry of Na^+ in addition to Ca^{2+} and the permeability to Na^+ varies from one channel to another (9 – 11). This implies that stimulation of GPCR can increase intracellular Na^+ concentration ($[Na^+]_i$) via cation channels possessing properties of NSCCs. In this regard, recent evidence suggests that Na^+ influx plays an important role in GPCR-mediated increase in $[Ca^{2+}]_i$. In isolated cardiac cells, stimulation of $G_{q/11}$ protein-coupled endothelin type A receptor (ET_AR) with its agonist endothelin-1 (ET-1) activates the Na^+/H^+ exchanger (NHE) via a PKC-dependent pathway, causing an increase in $[Na^+]_i$ that in turn drives the Na^+/Ca^{2+} exchanger (NCX) operating in the reverse mode to transport Ca^{2+} into cells in exchange for Na^+ efflux, leading to an increase in $[Ca^{2+}]_i$ (12 – 14). Moreover, activation of NHE by NA was observed in CHO cells expressing α_{1A}-AR (15), where mRNA expression for three members (NCX1, NCX2, and NCX3) of NCX was detected by RT-PCR (16). These raise the possibility that α_{1A}-AR modulates Na^+/Ca^{2+} exchange via increased Na^+ influx through NSCCs or NHE, resulting in an increase in $[Ca^{2+}]_i$.

The present study attempted to elucidate the mechanisms for NA-induced increase of $[Ca^{2+}]_i$ in CHO cells expressing human α_{1A}-AR using inhibitors for $G_{q/11}$ protein-regulated signaling molecules, cation channels, and transporters. In addition, the functional significance of Na^+ entry and NCX in the NA-induced $[Ca^{2+}]_i$ elevation were also examined using reduction of extracellular Na^+ concentrations and KB-R7943, an inhibitor of NCX, respectively.

Materials and Methods

Materials

The pCR3 mammalian expression vector containing human α_{1A}-AR cDNA was kindly provided by Dr. Ikunobu Muramatsu (Fukui University, Japan).

YM-254890 and LOE 908 ((R,S)-(3,4-dihydro-6,7-dimethoxy-isoquinoline-1-yl)-2-phenyl-N,N-di-[2-(2,3,4-trimethoxyphenyl)ethyl]-acetamide) were kindly pro-

vided by Astellas Pharma, Inc. (Tokyo) and Nippon Boehringer Ingelheim Co., Ltd. (Hyogo), respectively.

(−)-Noradrenaline (+)-bitartrate, 5-(N-ethyl-N-isopropyl)amiloride (EIPA), amiloride, lanthanum (III) chloride, G418, and probenecid were purchased from Sigma-Aldrich (St. Louis, MO, USA). Bisindolylmaleimide I (BIS I, 2-[1-(3-dimethylaminopropyl)-1H-indol-3-yl]-3-(1H-indol-3-yl)-maleimide), U-73122 (1-[6-((17β-3-methoxyestra-1,3,5(10)-trien-17-yl)amino) hexyl]-1H-pyrrole-2,5-dione), SK&F 96365 (1-[β-[3-(4-methoxyphenyl) propoxy]-4-methoxyphenethyl]-1H-imidazole), and KB-R7943 (2-(2-(4-(4-nitrobenzyloxy) phenyl)ethyl)isothiourea) were from Calbiochem (San Diego, CA, USA). Fura-2/acetoxymethyl ester (fura-2/AM), fluo-3/AM, and Pluronic F-127 were from Dojindo Laboratories (Kumamoto). The other regents used were of the highest grade in purity.

Cell culture

CHO cells were cultured in Ham's F-12 medium supplemented with 10% fetal calf serum, penicillin, and streptomycin and maintained at 37°C in humidified air with 5% CO_2.

Stable expression of human α_{1A}-AR in CHO cells

The pCR3 mammalian expression vector containing human α_{1A}-AR cDNA was transfected into CHO cells using a TransIT™-CHO transfection kit (Mirus Bio Corporation, Madison, WI, USA) according to the manufacturer's instructions. Transfected cells were selected using resistance to 800 $\mu g \cdot ml^{-1}$ G418.

Measurement of $[Ca^{2+}]_i$

$[Ca^{2+}]_i$ was measured as described previously (16). Briefly, CHO cells were incubated with 4 μM fura-2/AM or 10 μM fluo-3/AM admixed with 2.5 mM probenecid and 0.04% Pluronic F-127 at 37°C for 45 min under reduced light. After collecting and washing cells, the cells were suspended in Ca^{2+}-free Krebs-HEPES solution (140 mM NaCl, 3 mM KCl, 1 mM $MgCl_2 \cdot 6H_2O$, 11 mM D-(+)-glucose, 10 mM HEPES; adjusted to pH 7.3 with LiOH) at 4 × 10^5 cells/ml. $CaCl_2$ was added to 0.5-ml aliquot of the cell suspension at the final concentration of 1 mM, when necessary. Changes of $[Ca^{2+}]_i$ in cells were measured at 25°C using a CAF-110 spectrophotometer (JASCO, Tokyo) with the excitation wavelengths of 340 and 380 nm and emission wavelength of 500 nm for fura-2 and the emission wavelength of 540 nm and the excitation wavelength of 490 nm for fluo-3.

In the experiments with EIPA and amiloride, $[Ca^{2+}]_i$ was measured using fluo-3 instead of fura-2 because these drugs at the concentrations used in the present

study was found to interfere with the fluorescence signals of fura-2 (data not shown).

Data analyses

Data were collected and analyzed using a MacLab/8s and Chart (v. 3.5) software (ADInstruments Japan, Tokyo). The concentration-response curves for NA were constructed to evaluate its EC_{50} value, which is the effective NA concentration eliciting a half-maximal response, using GraphPad PRISM™ (version 3.00; GraphPad Software, San Diego, CA, USA). The concentration-inhibition curves were also obtained with GraphPad PRISM™ in order to estimate the IC_{50} values, which are the concentrations producing 50% inhibition of the control response. The EC_{50} and IC_{50} values were converted to logarithmic values (pEC_{50} and pIC_{50}) for analysis. Data are presented as means ± S.E.M., where n refers to the number of experiments. The significance of the difference between mean values was evaluated with GraphPad PRISM™ by one-way analysis of variance (ANOVA) followed by Tukey's multiple comparison test. A P value less than 0.05 was considered to indicate significant differences.

Results

Characterization of NA-induced transient and sustained increases in $[Ca^{2+}]_i$

Figure 1A shows a representative trace illustrating NA (1 μM)-induced increase in $[Ca^{2+}]_i$ in CHO cells stably expressing human α_{1A}-AR. NA elicited concentration-dependent increases in $[Ca^{2+}]_i$ that consist of an initial transient phase and a subsequent sustained phase

(Fig. 1B). The maximum increases in $[Ca^{2+}]_i$ by NA and its pEC_{50} values were 149.1 ± 5.1 nM and 7.56 ± 0.05 for the transient phase and 108.1 ± 1.5 nM and 7.39 ± 0.05 for the sustained phase, respectively (n = 6 for each). The NA (1 μM)-induced transient and sustained $[Ca^{2+}]_i$ increases were markedly reduced by removal of Ca^{2+} from the medium (the residual component of transient phase, 27.3 ± 3.4%; sustained phase, 17.0 ± 1.3%, n = 6 for each; Fig. 1C).

Pharmacological identification of Ca^{2+} channels involved in the transient and sustained increases in $[Ca^{2+}]_i$ in response to NA

To pharmacologically identify Ca^{2+} channels involved in the NA-induced increases in $[Ca^{2+}]_i$, we examined the effects of several Ca^{2+} channel blockers on the NA-induced transient and sustained increases in $[Ca^{2+}]_i$. Nifedipine, an inhibitor of L-type voltage-operated Ca^{2+} channel (VOCC), at concentrations up to 30 μM had no effect on the NA-induced Ca^{2+} responses (Fig. 2A). However, the NA-induced transient and sustained increases in $[Ca^{2+}]_i$ were concentration-dependently inhibited by SK&F 96365, an inhibitor of SOC and NSCC-2 (17), and LOE 908, an inhibitor of NSCC-1 and NSCC-2 (17) (Fig. 2: B and C). The inhibitory effects of these compounds at 30 μM on the transient and sustained phases were 79.4 ± 4.5% and 100.2 ± 1.7% for SK&F 96365 (n = 5) and 92.0 ± 1.1% and 91.3 ± 0.9% for LOE 908 (n = 5), respectively. Moreover, the transient and sustained increases in $[Ca^{2+}]_i$ triggered by NA were sensitive to La^{3+} (Fig. 2D), which is reported to inhibit certain members of the TRPC subfamily (3); and the inhibitory effects at 100 μM were 61.9 ± 4.4%
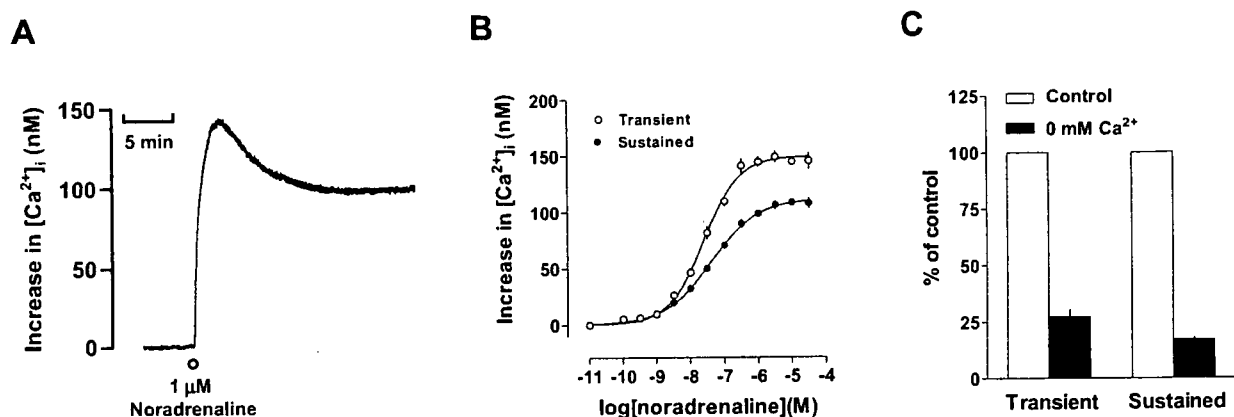
A   **B**   **C**

Fig. 1. Characterization of the NA-induced increase in $[Ca^{2+}]_i$ in the CHO cells stably expressing human α_{1A}-AR. $[Ca^{2+}]_i$ was measured using the Ca^{2+} indicator fura-2. A: A typical trace illustrating the $[Ca^{2+}]_i$ increases induced by NA (1 μM) in the presence of 1 mM Ca^{2+}. B: Concentration-response curves for the NA-induced transient and sustained $[Ca^{2+}]_i$ increases (n = 6). C: Effects of removal of extracellular Ca^{2+} on the transient and sustained phases generated by 1 μM NA (n = 6). The maximum $[Ca^{2+}]_i$ level induced by 1 μM NA for each phase in the presence of 1 mM Ca^{2+} was set to 100% as a control. Data are presented as means ± S.E.M. of the results obtained from n separate experiments.
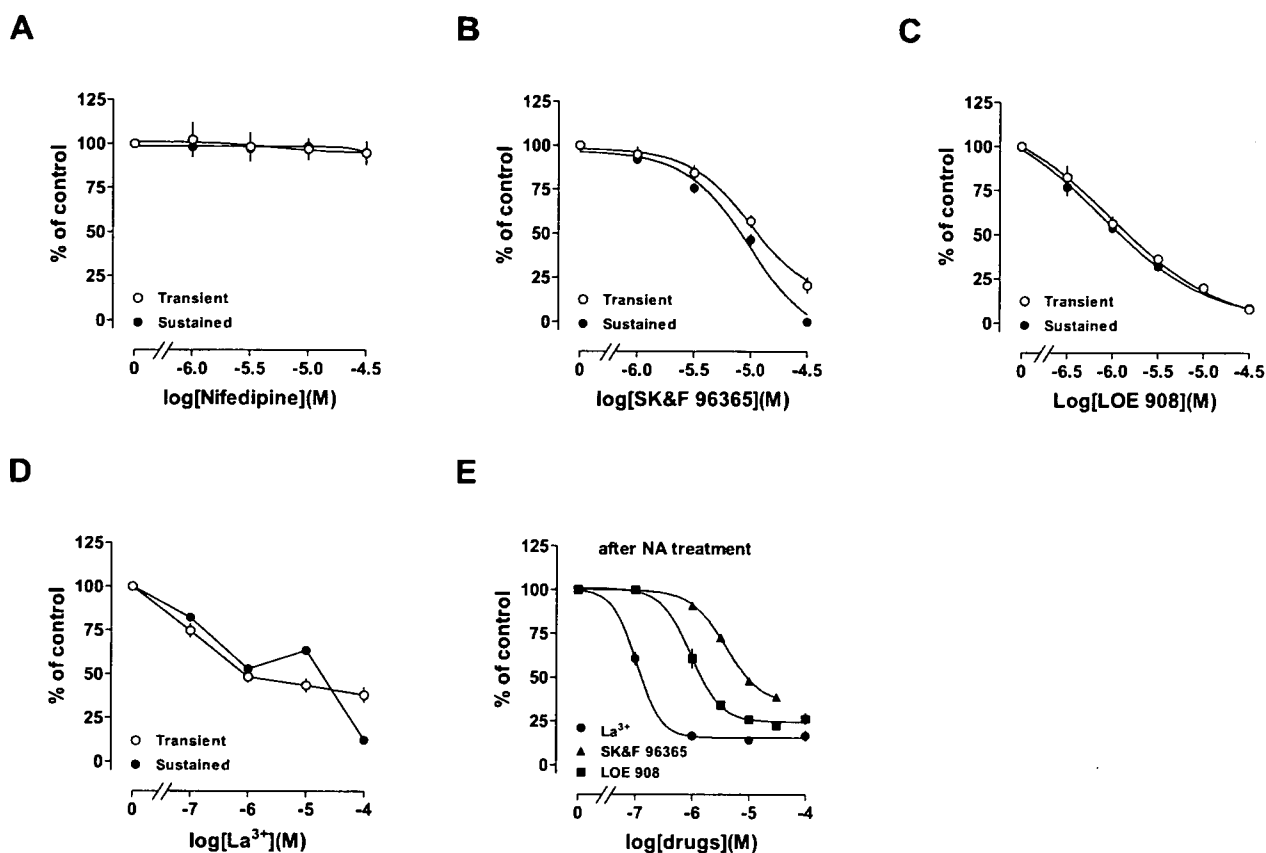
Fig. 2. Effects of pretreatment or post-treatment with cation channel blockers (nifedipine (A), SK&F 96365 (B, E), LOE 908 (C, E) and La^{3+} (D, E)) on the transient and sustained increases in [Ca^{2+}]$_i$ induced by 1 μM NA. These drugs were added 5 min before stimulation with NA (A – D) or during the sustained phase after stimulation with NA (E). The maximum [Ca^{2+}]$_i$ level induced by 1 μM NA for each phase in the presence of 1 mM Ca^{2+} was set to 100% as a control. Data are presented as means ± S.E.M. of the results obtained from 5 separate experiments.

and 87.8 ± 1.9%, respectively (n = 5). To further characterize the NA-induced sustained [Ca^{2+}]$_i$ increase, SK&F 96365, LOE 908, and La^{3+} were added after NA treatment. Figure 2E shows that the sustained phase was concentration-dependently suppressed by these inhibitors after NA treatment.

Importance of Na$^+$ influx in the NA-induced increases in [Ca^{2+}]$_i$

It is generally accepted that ROCs and SOCs allow the entry of Na$^+$ in addition to Ca^{2+}, resulting in an increase in [Na$^+$]$_i$ (9). However, the functional significance of Na$^+$ influx through these channels in the NA-induced increase in [Ca^{2+}]$_i$ is not well-known. To determine the role of Na$^+$ influx in the Ca^{2+} response to NA, the effects of reduction of extracellular Na$^+$ concentrations ([Na$^+$]$_e$) were tested. For this purpose, the [Na$^+$]$_e$ (140 mM) in normal Krebs-HEPES solution was reduced by replacing NaCl with equimolar LiCl. As shown in Fig. 3: A and B, the NA-induced transient and sustained increases in

[Ca^{2+}]$_i$ in normal Krebs-HEPES solution was unaffected by reducing [Na$^+$]$_e$ to 70 mM, but significantly suppressed by further reduction to either 10 or 0 mM. The inhibitory effects of reducing [Na$^+$]$_e$ to 0 mM on the transient and sustained phases were about 40% and 60%, respectively (n = 5), when compared with the responses in normal Krebs-HEPES solution containing 140 mM Na$^+$. These results suggest that Na$^+$ influx plays an important role in the transient and sustained [Ca^{2+}]$_i$ increases in response to NA.

In cardiac cells, stimulation of ET$_A$R with ET-1 activates the Na$^+$/H$^+$ exchanger (NHE), causing an increase in [Na$^+$]$_i$ as well as intracellular alkalinization (18). In addition, amiloride-sensitive Na$^+$ channel is reported to participate in extracellular Na$^+$ influx (19). To determine whether these Na$^+$ entry pathways are involved in the NA-induced increases in [Ca^{2+}]$_i$, the effects of EIPA, an inhibitor of NHE (13), and amiloride, an inhibitor of amiloride-sensitive Na$^+$ channel (20), were examined. However, the transient and sustained [Ca^{2+}]$_i$ increases in